

Investigation of Active Flow Control on an Extremely Thick Wind Turbine Airfoil

By

Kanin Homsrivanon

Submitted to the graduate program in Aerospace Engineering and the Graduate Faculty of the University of Kansas in partial fulfillment of the requirements for the degree of Master of Science.

Committee Chair: Dr. Saeed Farokhi

Committee Member: Dr. Ray Taghavi

Committee Member: Dr. Shawn Keshmiri

Date Defended: 05/12/2016

The Thesis Committee for Kanin Homsrivaranon certifies that this is the approved
version of the following thesis:

Investigation of Active Flow Control on an Extremely Thick Wind Turbine Airfoil

Committee Chair: Dr. Saeed Farokhi

Date Approved: 05/12/2016

Abstract

Today, modern wind turbine size has become larger than ever. The conventional airfoil near rotor hub cannot provide the structure integrity for the rotor blades. Large diameter wind turbine required for extremely thick airfoil, such as the FX77-W-343 34.4% wind turbine dedicated airfoil. The exceptionally thick airfoil has an unfavorable characteristic, such as sharp stalling and stalling at low angle of attack. To prevent undesired behavior, the FX77-W-343 airfoil with co-flow jet active flow control is simulated in 2-D CFD using STAR-CCM+ to investigate the enhancement in performance. The simulation is done at low Reynolds number of 1,000,000 with injection and suction momentum coefficient of 0.05. The simulation presents promising performance increase of maximum lift coefficient by 190% and improves lift-to-drag ratio by 94%. While sharp stalling behavior cannot be solved with co-flow jet flow control, the operating margin of the extremely thick airfoil is increased by 130% by delaying the stall angle of attack of 8deg.

Table of Contents

| | Page # |
|--|--------|
| Abstract | iii |
| Table of Contents | iv |
| List of Figures | v |
| List of Table | vii |
| List of Symbols | viii |
| 1 Introduction | 1 |
| 1.1 General Wind Turbine | 1 |
| 1.2 Literature Review | 3 |
| 1.3 Scope of Thesis | 6 |
| 2 Theoretical Consideration | 7 |
| 2.1 Sectional Lift and Drag Coefficients | 7 |
| 2.2 Injection and Suction Momentum Coefficient | 7 |
| 2.3 Reynolds Number | 7 |
| 2.4 Vorticity | 8 |
| 3 Computational Modeling and Validation | 9 |
| 3.1 Geometry | 9 |
| 3.2 Mesh Generation | 10 |
| 3.3 Physics Model | 11 |
| 3.4 Validation Case | 12 |
| 4 Results and Discussion | 17 |
| 4.1 Baseline FX77-W-343 | 17 |
| 4.2 Co-Flow Jet Modified FX77-W-343 | 23 |
| 5 Conclusion and Recommendation | 36 |
| 6 Reference | 37 |

List of Figures

| | Page # |
|---|--------|
| Figure 1: (Left) Dutch Windmill (Right) American Farm Windmill [6]..... | 1 |
| Figure 2: Size Comparison between Siemens D7 and Airbus A380 [4]..... | 2 |
| Figure 3: Lift and Drag Coefficient with Boundary Layer Leading Edge Suction by Hansen [11] | 3 |
| Figure 4: The Effect of Coanda Jet Location on Lift-to-Drag Ratio by Djodihardjo and Hamid [7]..... | 4 |
| Figure 5: Experimental and Numerical Comparison of Lift Coefficient versus AoA [6] | 5 |
| Figure 6: NACA0025 with Modified CFJ Airfoil [17]..... | 6 |
| Figure 7: 3 Dimensional Parallel Pipe Flow with Subtracted FX77-W-343 Airfoil | 9 |
| Figure 8: Generated Mesh on NREL S825 Airfoil for Validation Case..... | 13 |
| Figure 9: Smooth Transition between Prism Layer and Polyhedral Mesh on S825 Upper Wall . | 13 |
| Figure 10: Sectional Lift and Drag Coefficient on NREL S825 Airfoil (Validation Case) | 14 |
| Figure 11: Velocity Flow Field on NREL 825 at 0deg (left) and 14deg (right) AoA | 15 |
| Figure 12: Wall y^+ Value | 15 |
| Figure 13: Static Pressure Contour on NREL S825 Airfoil at 0deg (left) and 14deg (right) AoA | 16 |
| Figure 14: Vorticity Field on NREL S825 Airfoil at 0deg and 14deg AoA..... | 16 |
| Figure 15: Mesh Sensitivity on Sectional Force Coefficient | 17 |
| Figure 16: Mesh on FX77-W-343 Airfoil at 0deg AoA (Baseline Case)..... | 18 |
| Figure 17: Sectional Force Coefficients of FX77-W-343 Airfoil (Baseline Case) | 19 |
| Figure 18: Lift-to-Drag Ratio of FX77-W-343 Airfoil (Baseline Case)..... | 19 |
| Figure 19: Velocity Flow Field over FX77-W-343 Airfoil from -4deg to 12deg (baseline Case) | 21 |
| Figure 20: Static Pressure Contour on FX77-W-343 Airfoil at 0deg (right) and 10deg (right) AoA..... | 22 |
| Figure 21: Vorticity Field on FX77-W-343 Airfoil at 0deg and 6deg AoA..... | 23 |
| Figure 22: Co-Flow Jet Modified FX77-W-343 Airfoil Geometry (Left) and Mesh (right)..... | 24 |
| Figure 23: Injection and Suction Jet Momentum Coefficient versus Sectional Force Coefficient | 25 |

| | |
|---|----|
| Figure 24: Injection and Suction Jet Momentum Coefficient versus Lift-to-Drag Ratio | 25 |
| Figure 25: Sectional Force Coefficients Comparison between Baseline and Co-Flow Jet ($C\mu = 0.05$) | 27 |
| Figure 26: Lift-to-Drag Ratio Comparison between Baseline and Co-Flow Jet ($C\mu = 0.05$) | 27 |
| Figure 27: Co-Flow Jet Active Flow Control on FX77-W-343 Airfoil ($C\mu = 0.05$) | 29 |
| Figure 28: Static Pressure Contour on Modified FX77-W-343 airfoil at 0deg (left) and 16deg (right) AoA..... | 30 |
| Figure 29: Velocity Flow Field near Leading Edge (left) and Trailing Edge (right) of Co-Flow Jet Flow Control FX77-W-343 Airfoil at 6deg AoA..... | 30 |
| Figure 30: Vorticity Field near Leading Edge (top) and Trailing Edge (bottom) of Co-Flow Jet Flow Control FX77-W-343 Airfoil at 6deg AoA | 31 |
| Figure 31: Vorticity Field on Co-Flow Jet Flow Control FX77-W-343 Airfoil at 0deg (Top) and 16deg (bottom) AoA..... | 32 |
| Figure 32: Comparison of the Wake Structure with Various Injection and Suction Momentum Coefficient on Co-Flow Jet Flow FX77-W-343 airfoil at 6deg AoA..... | 33 |
| Figure 33: Comparison of the Wake Structure with Various Injection and Suction Momentum Coefficient on Co-Flow Jet Flow FX77-W-343 airfoil at 6deg AoA (continue) | 34 |
| Figure 34: Comparison between Velocity Field on Baseline (left) and Modified Co-Flow Jet (right) FX77-W-343 Airfoil at 6deg AoA | 35 |
| Figure 35: Comparison between Static Pressure Contour on Baseline (left) and Modified Co-Flow Jet (right) FX77-W-343 Airfoil at 6deg AoA..... | 35 |

List of Table

| | Page # |
|--|--------|
| Table 1: Mesh Setting in STAR-CCM+ | 11 |
| Table 2: Physics Model in STAR-CCM+..... | 11 |

List of Symbols

| <u>Symbol</u> | <u>Description</u> | <u>Units</u> |
|---------------------|--|--------------|
| A | Area..... | m^2 |
| $C_{l\alpha}$ | Lift Curve Slope..... | rad^{-1} |
| C_d | Sectional Drag Coefficient..... | ~ |
| C_l | Sectional Lift Coefficient..... | ~ |
| C_μ | Equivalent Jet Momentum Coefficient..... | ~ |
| C_p | Pressure Coefficient..... | ~ |
| c | Chord Length..... | m |
| D | Drag Force..... | N |
| L | Length..... | m |
| L | Lift Force..... | N |
| \dot{m} | Mass Flow Rate..... | kg/s |
| Re | Reynolds Number..... | ~ |
| t | Jet Thickness..... | m |
| V | velocity..... | m/s |
| y^+ | Wall y^+ | ~ |
| α | Angle of Attack..... | deg |
| μ | Dynamic viscosity..... | Pa-s |
| ω | Vorticity..... | /s |
| ρ | Density..... | kg/m^3 |

| <u>Subscripts</u> | <u>Description</u> |
|-------------------|--------------------|
| ∞ | Freestream |
| d | Drag |
| l | Lift |
| max | Maximum |
| ref | Reference |

| <u>Acronym</u> | <u>Description</u> |
|-----------------------|---|
| AoA..... | Angle of Attack |
| CFD..... | Computational Fluid Dynamic |
| CFJ | Co-Flow Jet |
| NACA | National Advisory Committee for Aeronautics |
| NREL | National Renewable Energy Laboratory |
| RANS | Reynolds-Average Navier-Stokes |
| SST..... | Shear Stress Transport |
| VG..... | Vortex Generator |

1 Introduction

1.1 General Wind Turbine

The wind turbine technology has been used for a very long period of time. Persians used the first wind turbine, known as the “Persian windmill” or “Panemone”, for grain grinding through aerodynamic drag force. In the 16th century, the Europeans extracted wind energy through the Dutch windmill for grinding wheat. The farms in America used steel-bladed wind turbines to pump water and grind wheat in the 18th century. Today, the primary use of the wind turbine is to extract wind energy to generate electricity.



Figure 1: (Left) Dutch Windmill (Right) American Farm Windmill [6]

Over the years, the wind turbine designs have been studied to increase its performance. There are many factors contributing to wind turbine performance and efficiency. One of the very important aspects of wind turbine design is the airfoil shape of the rotor blades. The wind turbine blade design was first borrowed from the airfoil shape of the airplane, such as the NACA airfoil series, for its lift characteristic, though it was later realized that the two systems operate in different conditions. Airplanes typically operate at high altitudes in which the wing surface stays clean, while the wind turbine operates closer to the ground and experiences dirt, insects, and

other environmental debris. The environmental factors introduce the surface roughness to the shape of the airfoil and therefore reduce the aerodynamic efficiency. Many organizations have studied and designed wind turbine specific aerodynamic shapes that are less sensitive to the surface roughness while maintaining high lift-to-drag ratio. Delft University, National Renewable Energy Laboratory (NREL), and FFA and RISO are some of the institutes that came up with the airfoil series specifically tailored for extracting wind energy into electricity.

Aside from the efficiency standpoint, the design of modern wind turbine also has tremendously increased in size. For instance, the Siemens 7MW D7 platform direct-drive and AMSC SeaTitan 10 MW wind turbines have the rotor diameter of 154m and 190m, respectively. Figure 2 shows size comparison between the Siemens D7 rotor size to Airbus A380. This modern design of a wind turbine rotor has become so large that the typical dedicated wind turbine airfoil, 15% to 25% thickness to chord ratio, cannot provide the structural integrity for such large configurations. Thus, the rotor hub airfoil required extremely thick airfoil, in the order of 35% to 45% thickness to chord ratio. Some of the examples of the wind turbine specific thick airfoils are Delft DU00-W2-xxx and Wortmann FX77-W-xxx series.

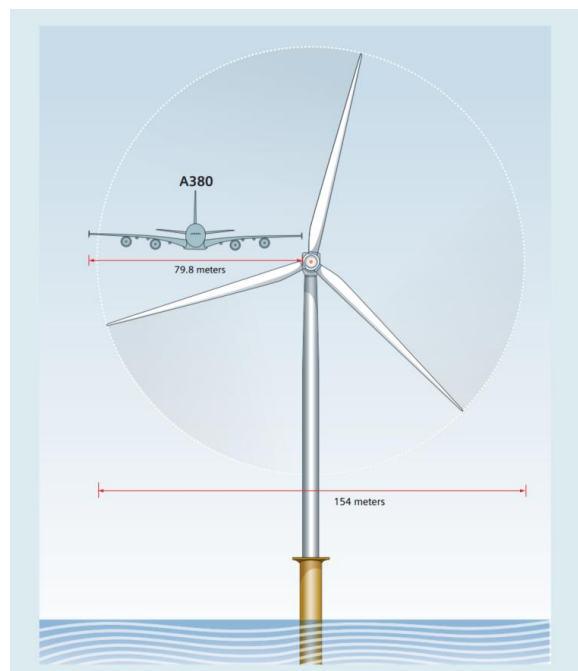


Figure 2: Size Comparison between Siemens D7 and Airbus A380 [4]

The extremely thick foils typically have undesirable aerodynamic characteristics such as sharp stalling behavior or stalling at low angle of attack (AoA). Many methods of controlling the flow over an airfoil, including passive and active control, have been developed over the years to enhance the performance of the aerodynamic body. An example of passive flow control is vortex generator (VG) and riblets. Similarly, jet flow injection and suction are normally used to actively control the flow field over the airfoil.

1.2 Literature Review

Based on the previous studies on active flow control, not much has been contributed to the extremely thick airfoil, though various types and configurations have been employed for conventional airfoil, as well as the wind turbine dedicated airfoil.

In 2010, Martin O.L. Hansen [11] conducted active flow control research on boundary layer suction for wind turbine airfoil using numerical method, Computational Fluid Dynamic (CFD). Hansen modeled NACA4415 in ANSYS CFX 12.1 with various suction slot configurations and simulated at different angles of attack to compute lift and drag coefficient. His research attempted to improve the aerodynamic performance of the airfoil at high AoA. It was concluded that the suction location is the most effective at the leading edge and a maximum lift coefficient increase of 20% can be expected over the clean baseline airfoil.

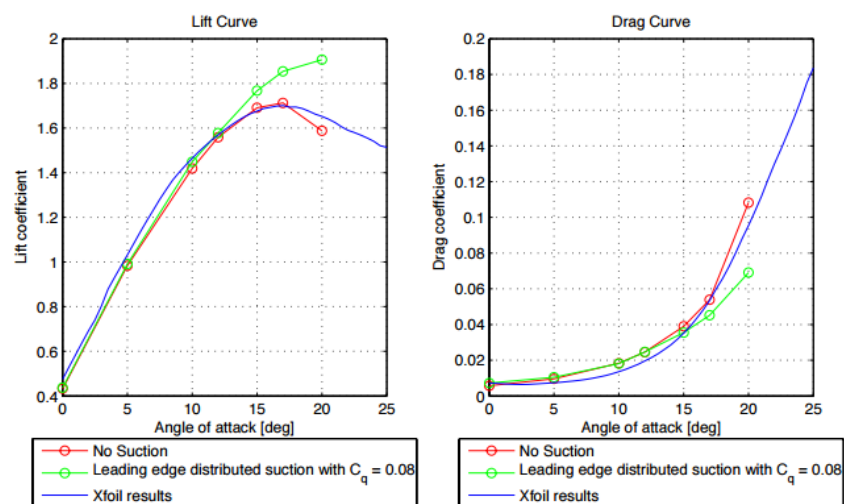


Figure 3: Lift and Drag Coefficient with Boundary Layer Leading Edge Suction by Hansen [11]

Djojodihardjo and Hamid [7] from the University Putra Malaysia investigated Coanda effect lift enhancement on wind turbine specific airfoil, particularly NREL S809 airfoil. The research is done in 2-D using CFD. The computation is conducted using Reynolds-Average Navier-Stokes (RANS) equations through commercially available software, COMSOL 4.2. To check the model validity in COMSOL, they ran the base model S809 airfoil against the experimental data and found it to be consistent. The authors modified the airfoil trailing edge to have various curvatures, ranging from 10mm to 50mm. The location of the Coanda jet outlet, from 90% to 95% of chord length, has also been studied in this paper. After the simulation of the S809 at 0deg angle of attack, it is confirmed that the Coanda circulation control airfoil does, in fact, enhance airfoil lift characteristics. The lift-to-drag ratio is found to be maximum when the trailing edge radius is 30mm, then decreases as the curvature enlarges from 30mm to 50mm. Lastly, the lift-over-drag ratio increases as it approaches the trailing edge zone.

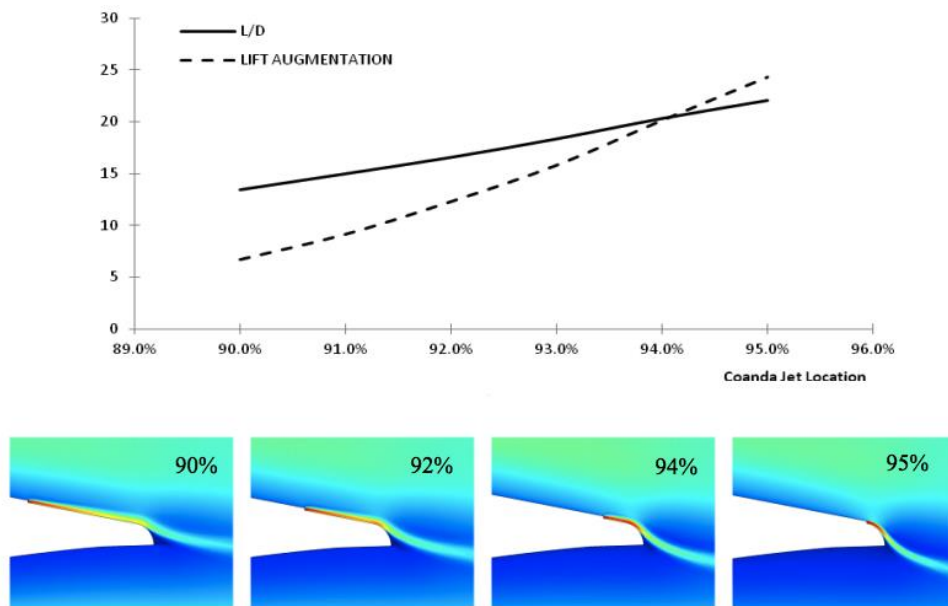


Figure 4: The Effect of Coanda Jet Location on Lift-to-Drag Ratio by Djojodihardjo and Hamid [7]

A group of engineers at the University of Miami and University of Florida conducted research on high performance airfoil using their own active flow control design, called “Co-Flow Jet (CFJ)” [16,17]. Their CFJ airfoil configuration consists of an air injection slot near the airfoil leading edge and a suction slot close to the trailing edge. Engineers implemented the co-flow jet

by modifying the upper surface of NACA0025 airfoil in both CFD and on a real wing to test in the wind tunnel. Experimental and numerical results both have shown to tremendously increase performance of the NACA0025 airfoil at high AoA. The engineers reported that the wind tunnel data shows an increase in lift coefficient ranging from 113% to 220%, an increase in operating range (stall margin) ranging from 100% to 153%, and a reduction in drag coefficient by at least 30%. The authors also claimed that the negative drag (or thrust) can be produced at high momentum coefficients of the injection and suction jet.

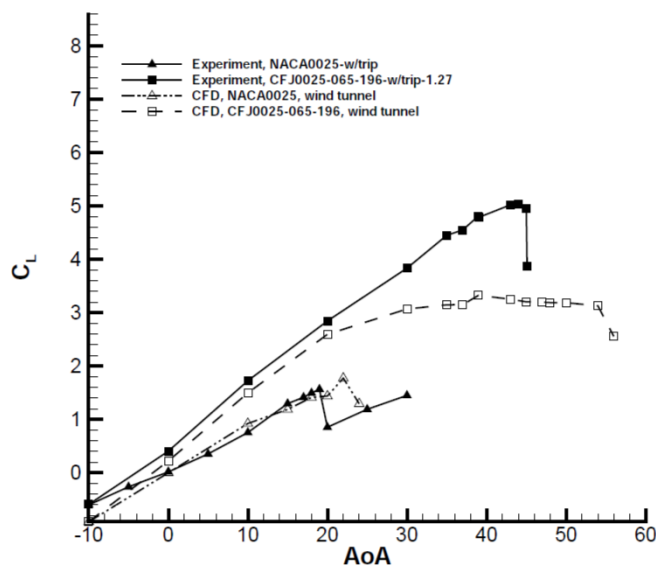


Figure 5: Experimental and Numerical Comparison of Lift Coefficient versus AoA [6]



Figure 6: NACA0025 with Modified CFJ Airfoil [17]

1.3 Scope of Thesis

This Master's thesis investigates the active flow control over an extremely thick wind turbine specific airfoil using STAR-CCM+. The airfoil selected is the Wortmann FX77-W-343, with a 34.4% thickness ratio, due to the availability of its airfoil coordinates. Following the literature review of the active flow control methodology, co-flow jet is selected to be suitable for enhancing the performance of an extremely thick airfoil primarily due to its capability to enhance lift-to-drag ratio and allowing the airfoil to stall at a much higher AoA. The airfoil will be simulated in 2-dimensions at a Reynolds number of 1,000,000 within STAR-CCM+, and this model will be validated with the wind tunnel experimental data. The mesh sensitivities will also be studied to refine mesh size and the number of elements inside the flow domain. Then, the active co-flow jet will be implemented on the top surface of FX77-W-343 series airfoil to be simulated and results will be compared to the baseline data.

2 Theoretical Consideration

2.1 Sectional Lift and Drag Coefficients

Lift coefficient (C_l) and drag coefficient (C_d) are non-dimensional parameters that represent the aerodynamic characteristic of airfoils, or any aerodynamic body. The 2-D sectional lift and drag coefficients are defined by the following.

$$C_l = \frac{L}{\left(\frac{1}{2}\right)\rho V_\infty^2 c} \quad (1)$$

$$C_d = \frac{D}{\left(\frac{1}{2}\right)\rho V_\infty^2 c} \quad (2)$$

L and D represents lift and drag forces in the above equations.

2.2 Injection and Suction Momentum Coefficient

In order to quantify the quantity of the air being injected or extracted from the incoming flow, the dimensionless parameters are used and called “equivalent jet momentum coefficients (C_μ)”. The parameters characterize the jet momentum by relating the incoming flow velocity and density to the injection and suction flow properties. In the 2-D case, the chord length (c) and jet thickness (t) are implemented instead of reference area (A_{ref}) of the injection and suction slot in 3D case. The injection and suction equivalent jet momentum are described by the following equations.

$$C_{\mu injection} = \frac{\dot{m}V_{injection}}{\left(\frac{1}{2}\right)\rho_\infty V_\infty A_{ref}} = \frac{\rho_{injection} V_{injection}^2 t_{injection}}{\left(\frac{1}{2}\right)\rho_\infty V_\infty^2 c_{airfoil}} \quad (3)$$

$$C_{\mu suction} = \frac{\dot{m}V_{suction}}{\left(\frac{1}{2}\right)\rho_\infty V_\infty A_{ref}} = \frac{\rho_{suction} V_{suction}^2 t_{suction}}{\left(\frac{1}{2}\right)\rho_\infty V_\infty^2 c_{airfoil}} \quad (4)$$

2.3 Reynolds Number

Reynolds number is another dimensionless parameter and is the ratio of inertial force to viscous force. The Reynolds is defined by the following equation.

$$Re = \frac{\rho V_\infty L}{\mu} \quad (5)$$

By the above equations, L represents length scale and μ is dynamic viscosity.

2.4 Vorticity

Vorticity is a parameter that described the rotational motion of the fluid flow. According to Shapiro [14], the vorticity is a curl of velocity vector that can be expressed by the following formula.

$$\omega = \nabla \times \bar{u} \quad (6)$$

3 Computational Modeling and Validation

3.1 Geometry

The FX77-W-343 airfoil coordinates are taken from University of Illinois Urbana-Champaign (UIUC) Applied Aerodynamics Group [1] airfoil database. These coordinates are imported into NX 8.5 and connected by spline curves, upper and lower curves. The airfoil has chord length of 1m and was extruded to give a thickness of 0.2m. This sectional 3-D airfoil is exported as a Parasolid part file. The reason the airfoil sketch has to be extruded is due to the fact that STAR-CCM+ operates in 3-D space. The method to simulate this airfoil in 2-D will later be explained. The creation of the co-flow jet airfoil modified version of FX77-W-343 is also done exactly the same way as explained above with the revised top surface for injection and suction slots.

In STAR-CCM+, the Parasolid file of the airfoil can be imported to create the flow domain. The flow field, air-box liked shaped, can be created by drawing connected straight line then extrude with 0.2m thickness. The flow domain has dimensions of 20m x 25m. The inlet is 10m ahead of the leading edge of the airfoil and outlet is located 14m behind the trailing edge, as can be seen in Figure 7. Then, the flow domain is completed by Boolean subtracting the airfoil from air-box construction.

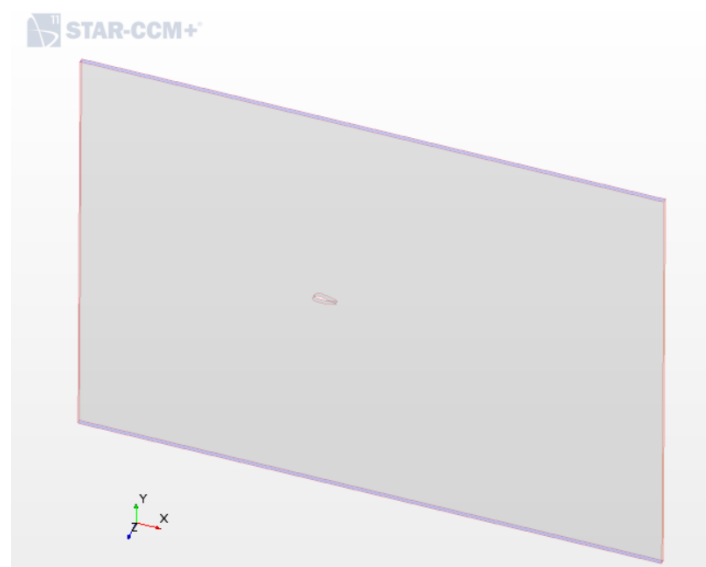


Figure 7: 3 Dimensional Parallel Pipe Flow with Subtracted FX77-W-343 Airfoil

3.2 Mesh Generation

To generate 2-D mesh, the 3-D parallel air-box flow is executed with 2-D badge operation. This process allowed for the creation of 2-D mesh with one element thickness. Each surface in the flow domain is then assigned into different boundary types. Inlet and outlet are designated as velocity inlet and pressure outlet, respectively. Top and bottom walls are selected to be symmetrical walls. The airfoil itself is chosen to be a solid wall. In the case of co-flow jet modified airfoil, the injection and suction surface are assigned to be inlet and outlet with quantified velocity normal to surface plane to control the flow jet that is being injected or extracted from the flow field.

Now, the flow field is ready for the mesh operation. The mesh type is selected to be polyhedral with prism layer mesher. The polyhedral mesh has significant advantages over tetrahedral, as it allowed for fewer cells and much smoother growth away from the body. Less element inside the flow field means faster computing time. Also suggested by Penny [10], polyhedral mesh is typically preferred in aerodynamic study when force coefficient is the key important parameter. The prism layer mesh is used at near wall region to capture the boundary layer flow field. It is important that the boundary layer thickness is a tall enough height to cover the boundary layer. Smooth transition between the two types of mesher is another key to achieving good force coefficient results. The following table represented the selected mesh types, values and custom controls applied in STAR-CCM+.

Table 1: Mesh Setting in STAR-CCM+

| Mesher | |
|---|--------------------|
| Mesh Type | Polygonal Mesher |
| | Prism Layer Mesher |
| Mesh Values | |
| Target Surface Size (m) | 0.006 |
| Minimum Surface Size (m) | 0.0001 |
| Surface Growth Rate | 1.1 |
| Number of Prism Layers | 40-60 |
| Prism Layer Stretching | 1.2 |
| Prism Layer Total Thickness (m) | 0.02 |
| Surface Control on Leading and Trailing Edge | |
| Target Surface Size (m) | 0.004 |
| Wake Refinement Control on Airfoil | |
| Relative Size (m) | 0.02 |
| Wake Refinement Distant (m) | 8 |
| Custom Control on Inlet, Outlet and Symmetry Walls | |
| Target Surface Size (m) | 0.75m |

3.3 Physics Model

Table 2 shows the selected physics model that will be used throughout the 2-D airfoil simulation cases in this report.

Table 2: Physics Model in STAR-CCM+

| Physics Model | |
|------------------------------------|--|
| Space | 2 Dimensional |
| Time | Steady |
| Flow | Segregated Flow |
| Material | Gas |
| Equation of State | Constant Density |
| Viscous Regime | Turbulent |
| Turbulence Model | Reynolds-Average Navier-Stokes (RANS) |
| Reynolds-Average Turbulence | K-Omega Turbulence |
| K-Omega Turbulence Models | Shear Stress Transport (SST) K-Omega |
| K-Omega Wall Treatment | Low y^+ Wall Treatment (Y^+ Wall < 1) |
| Transition | Turbulence Suppression |
| Optional Model | Cell Quality Remediation |

The simulation is in steady-state with constant density gases. The constant air property is chosen to have the constant density of 1.1842kg/m^3 and dynamic viscosity of $1.8551\text{E-}5$ Pa-s.

Time-averaged incompressible RANS equations are chosen to govern the motion of the fluid flow. The govern RANS can be expressed by the following equation [9].

$$\rho \bar{u}_i \left(\frac{\partial \bar{u}_i}{\partial x_j} \right) = \rho \bar{f}_i + \frac{\partial}{\partial x} \left[-\bar{p} \delta_{ij} + \mu \left(\frac{\partial \bar{u}_i}{\partial x_j} + \frac{\partial \bar{u}_j}{\partial x_i} \right) - \rho \overline{u'_i u'_j} \right] \quad (7)$$

The SST $k-\omega$ turbulence model is a robust two-equation eddy-viscosity model that is suitable for low Reynolds number study and can be used to solve the model through sublayer down to the wall. The SST $k-\omega$ is widely used in the aerospace industry as it is performing well for swirling flows and adverse pressure gradients, or flow separation region [3].

The wall treatment is an assumption of near-wall modeling. Wall treatment is selected to be a low wall y^+ due to that fact that simulation of airfoil will be conducted at low Reynolds number. This low y^+ model is valid throughout the boundary and viscous sublayer. The requirement for this wall treatment is that prism layer mesh must be sufficiently fine, with value of less than 1 [5].

3.4 Validation Case

Due to the lack of experimental data on extremely thick airfoil (Wortmann FX77-W-343), a validation case will be simulated with a different wind turbine airfoil, NREL S825. The airfoil coordinates are found from NREL website [2]. S825 is a 17% thick airfoil and was tested by NASA Langley in 1999. The experimental wind tunnel data can be obtained in “Design and Experimental Results for the S825 Airfoil” by D.M. Somers, Airfoils, Inc. [15].

The validation case using NREL S825 wind turbine airfoil is conducted with mesh and physics model setting as described in previous sections of this document. The generated mesh of the S825 is shown in Figure 8. The flow domain consists of 57,235 elements with finer mesh size near the leading and trailing edge section. The mesh is much finer around the airfoil and smoothly grows larger to 0.75m at the boundary of the flow domain, as seen in Figure 9: Smooth Transition between Prism Layer and Polyhedral Mesh on S825 Upper Wall. The wake refinement of 8m can also be seen immediately behind the airfoil.

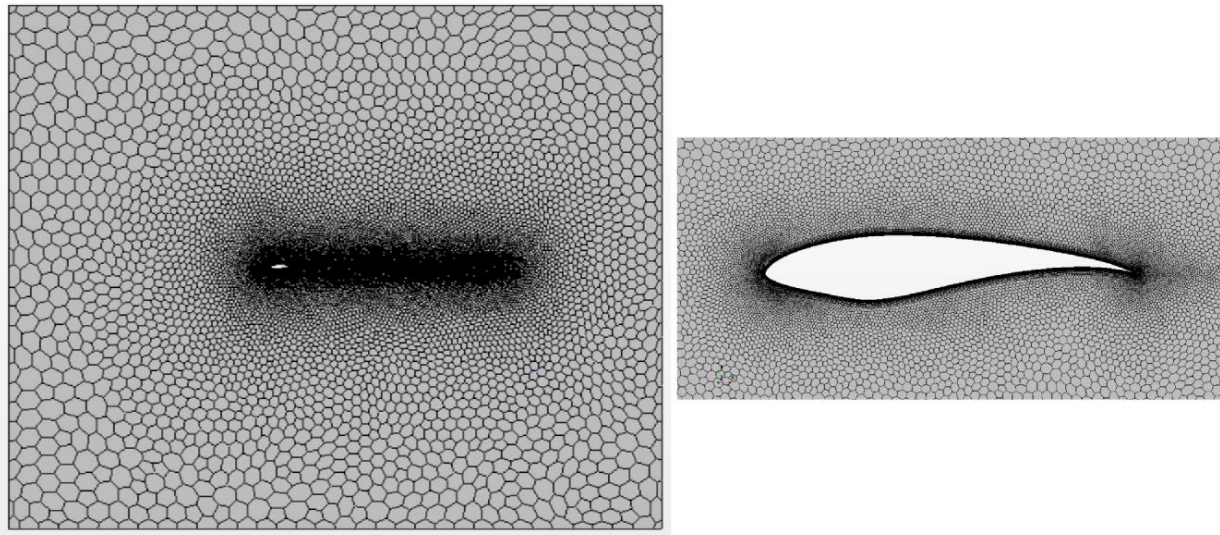


Figure 8: Generated Mesh on NREL S825 Airfoil for Validation Case

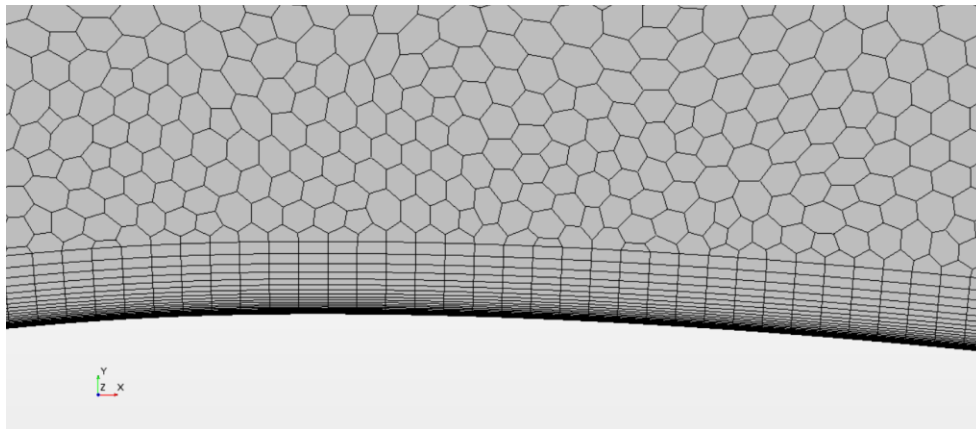


Figure 9: Smooth Transition between Prism Layer and Polyhedral Mesh on S825 Upper Wall

The NREL S825 is simulated in the constant density flow of 15.66m/s or Reynolds number of 1,000,000 from -2deg to 18deg AoA. Sectional lift and drag coefficients are collected and compared to the wind tunnel results. The STAR-CCM+ lift coefficients matched with the experimental data within 5% from -2 to 10deg AoA. Drag coefficients in 2-D case are more difficult to match than lift coefficient but are within 20% errors. Although the accuracy of drag is not as good, the STAR-CCM+ simulation still captured the drag behaviors of the S825 wind turbine airfoil. The force coefficients accuracy drop as the airfoil approaches the stall and post stall region but again still predicted $C_{l_{max}}$ at precisely 12deg AoA. The comparison between

wind tunnel experimental results and STAR-CCM+ data can be seen in Figure 10. The flow vector flow field around the airfoil at the AoA of 0deg and 14deg can be found in Figure 11. As expected, the flow velocity is higher on the upper contour of the airfoil that leads to lower pressure and resulting in upward force, or lift force. At AoA of 14deg the velocity field demonstrates flow separation at near trailing edge region.

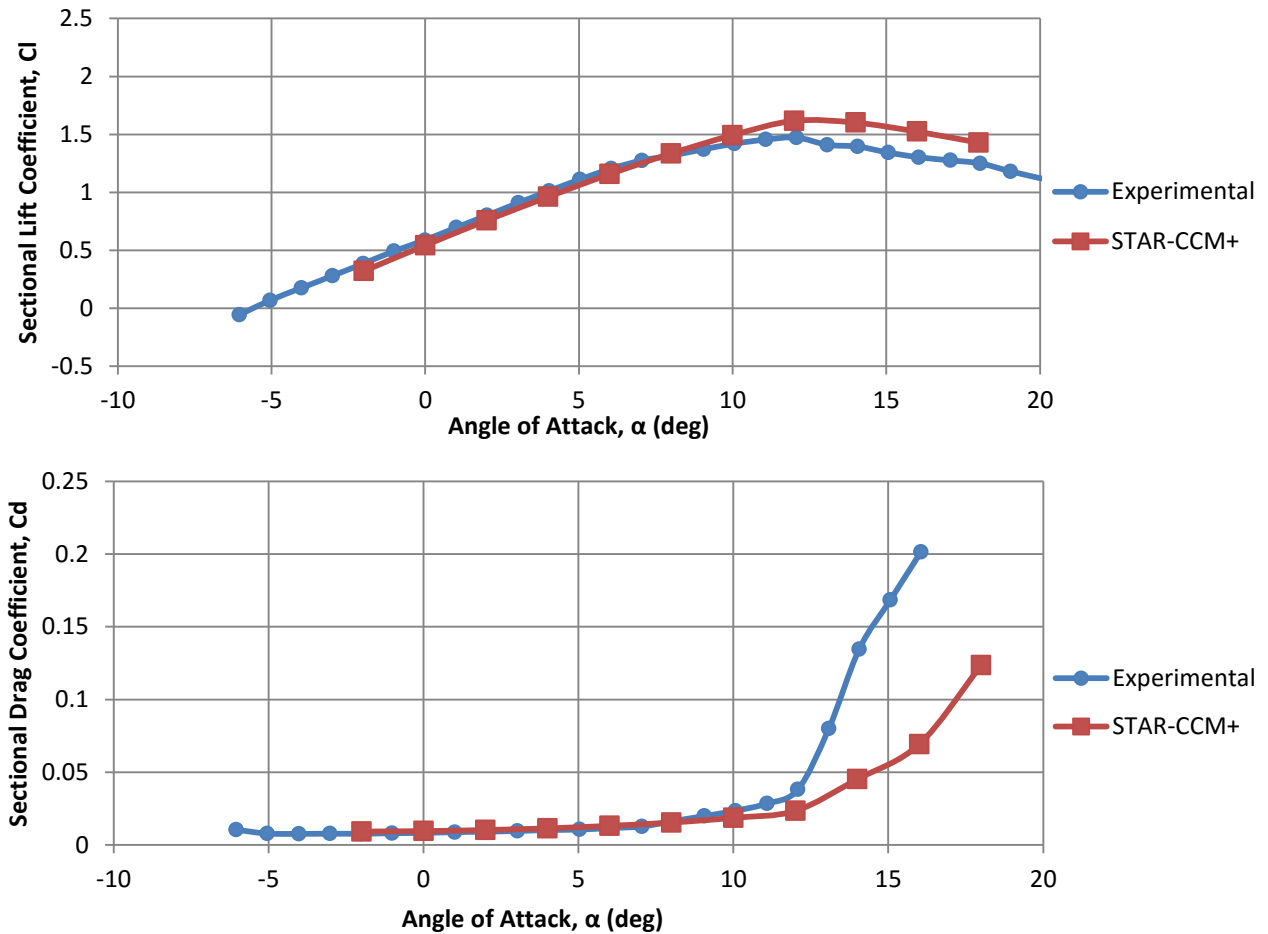


Figure 10: Sectional Lift and Drag Coefficient on NREL S825 Airfoil (Validation Case)

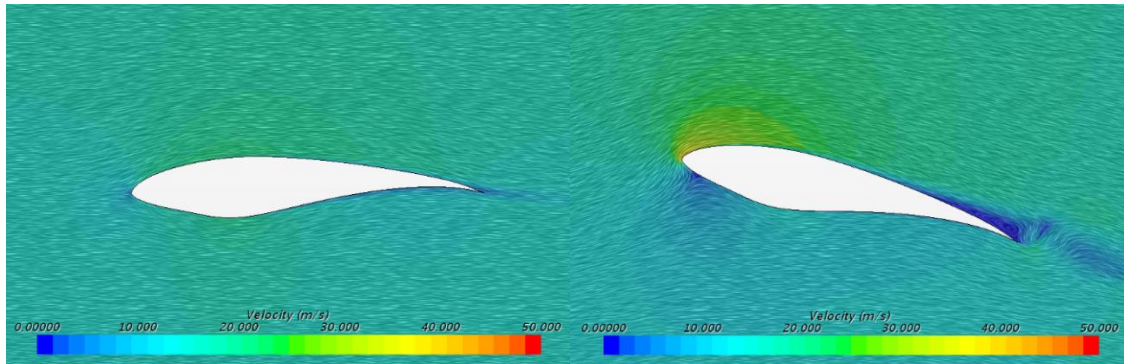


Figure 11: Velocity Flow Field on NREL 825 at 0deg (left) and 14deg (right) AoA

Following practices to achieving good CFD results, as described in previous section, the wall y^+ value on the wall is below 1 and can be seen in Figure 12.

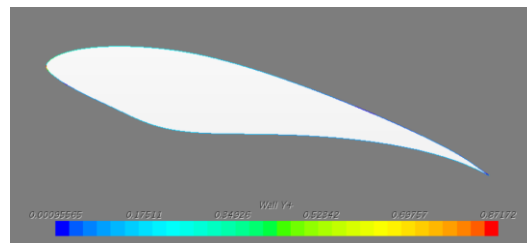


Figure 12: Wall y^+ Value

Figure 13 displays the static pressure contour on NREL S825 wind turbine dedicated airfoil at two different AoA. The two AoA cases show the static pressure on the upper region is higher than the lower region, but the difference between at 14deg is much larger than at 0deg AoA. This larger difference in pressure suggests that at 14deg AoA, the lift force must be higher. It can be confirmed by Figure 10 that lift coefficient of the S825 airfoil is higher at 16deg.

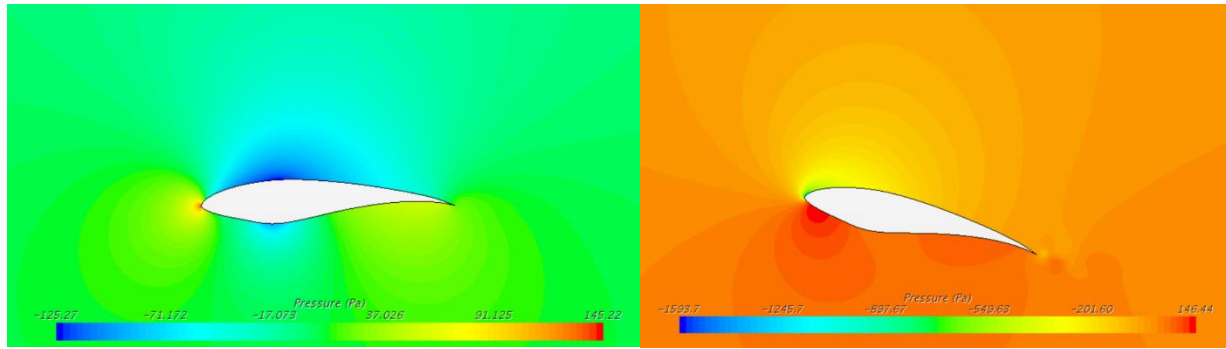


Figure 13: Static Pressure Contour on NREL S825 Airfoil at 0deg (left) and 14deg (right) AoA

Although the lift coefficient is higher at 14deg, the drag coefficient is lower at 0deg AoA. The wake behind an airfoil contributes to drag coefficient. As seen in the velocity field at 14deg AoA, flow separation appeared at the airfoil trailing edge. This separation of flow creates wake structure immediate aft of the airfoil body. The wake trail can be seen as a vorticity field, or rotation of the flow field. Figure 14 presents the vorticity field on S825 airfoil at 0deg and 14deg AoA. The thicker and stronger wake trail behind 16deg AoA leads to higher sectional coefficient of drag than 0deg AoA.

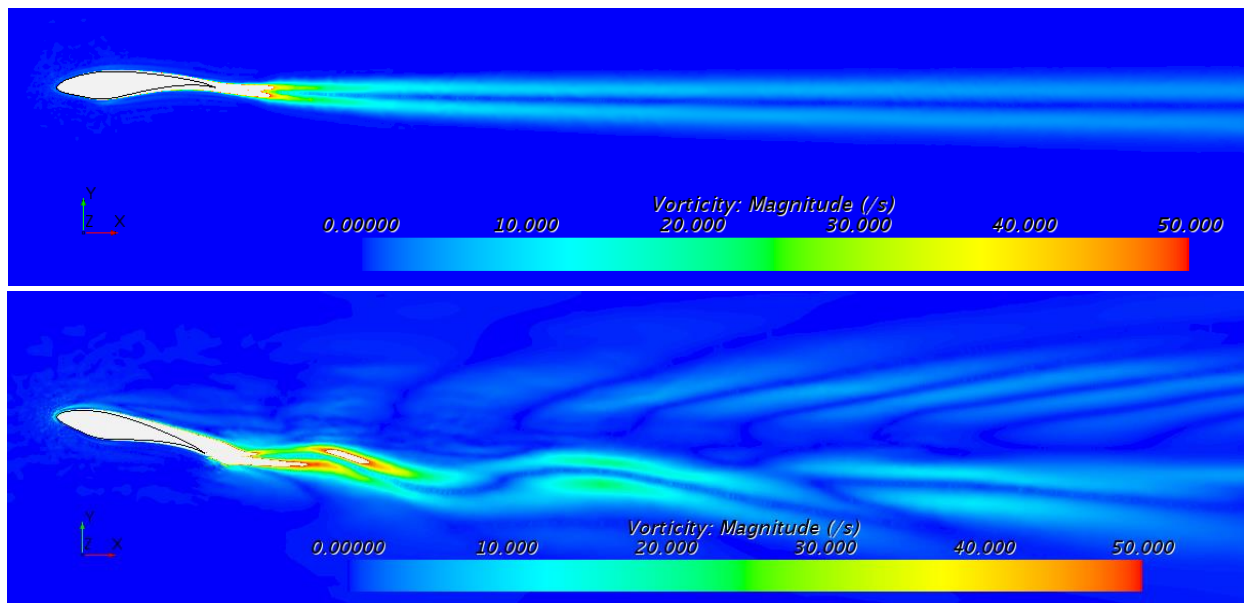


Figure 14: Vorticity Field on NREL S825 Airfoil at 0deg and 14deg AoA

4 Results and Discussion

This section of the Master’s thesis document presents the result and discussion of the baseline and modified FX77-W-343 extremely thick wind turbine airfoil.

4.1 Baseline FX77-W-343

The airfoil coordinates are obtained from UIUC airfoil data website and the airfoil model is created in STAR-CCM+ software following practices defined in chapter 3. Similar to the validation case, the baseline FX77-W-343 extremely thick wind turbine airfoil is simulated at Reynolds number of 1,000,000 from -4deg to 12deg AoA. Mesh sensitivity study is also implemented on the wind turbine dedicated FX airfoil at 0deg AoA and can be seen in Figure 15. The lift and drag coefficients value converges within 1% precision when the element counts in the flow domain reaches 50,000. Although the exact number of the element inside the flow domain cannot be controlled due to limitation in mesh setting, Figure 15 ensured that the force coefficients results will not deviate more than 1% when element is above 50,000.

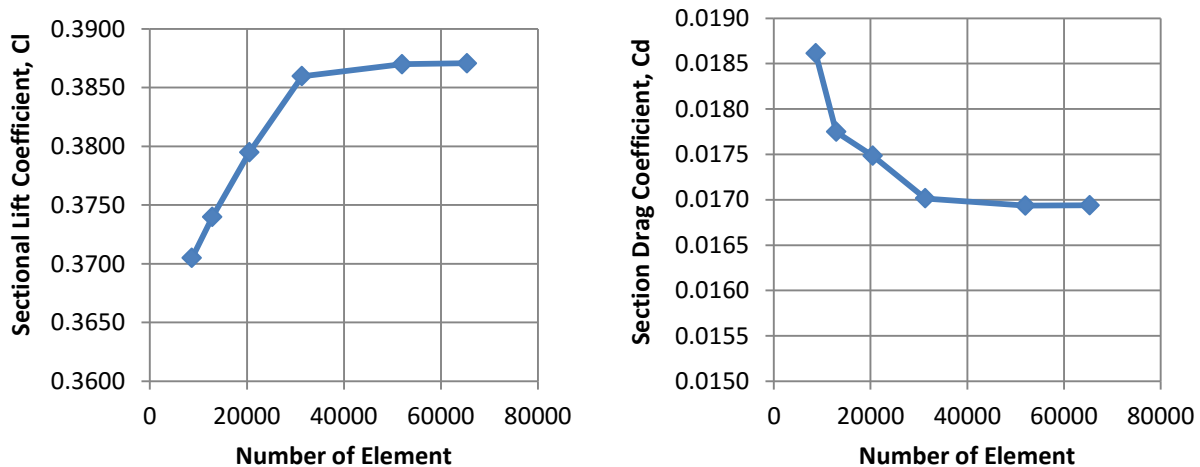


Figure 15: Mesh Sensitivity on Sectional Force Coefficient

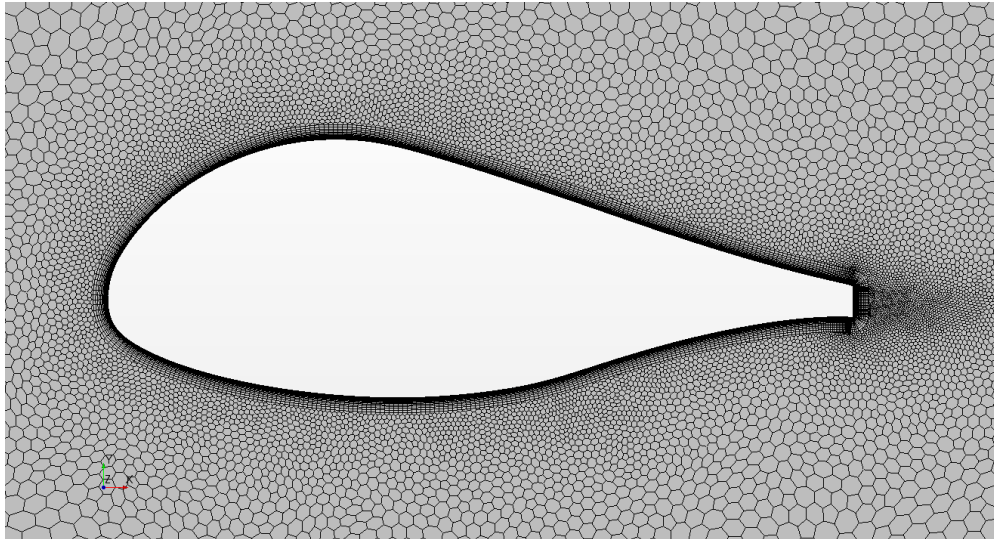


Figure 16: Mesh on FX77-W-343 Airfoil at 0deg AoA (Baseline Case)

Following the mesh sensitivity study, all of the simulation for baseline FX77-W-343 airfoil is setup to have mesh element of at least 50,000. The aerodynamic performance of the extremely thick wind turbine airfoil is studied at the Reynolds number of 1,000,000 and can be viewed in Figure 17. Based on the results from STAR-CCM+, the 34.4% thick airfoil stalls at 6deg AoA with $c_{l_{max}}$ of 0.82. The linear range of the lift curve slope ($C_{l_{\alpha}}$), from -2deg to 4deg AoA, is determined to be 6.176rad^{-1} . On the other hand, drag coefficient begins to rise tremendously after 4deg AoA. Lift-to-drag ratio is another important efficiency parameter to the performance of the lifting aerodynamic surface. The baseline thick airfoil is capable of producing maximum lift-to-drag ratio of 30 at 2deg AoA.

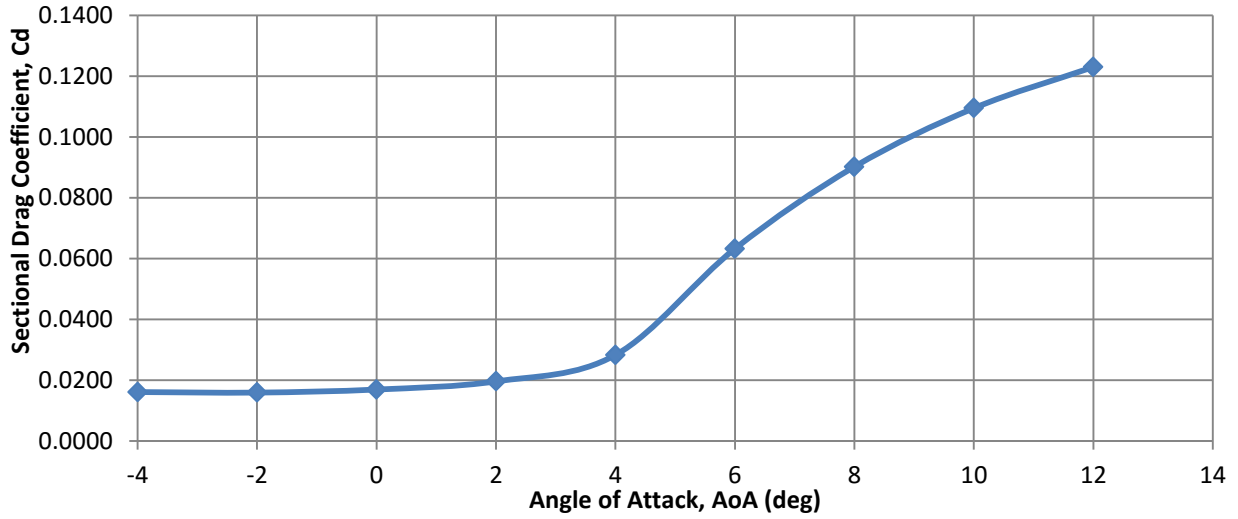
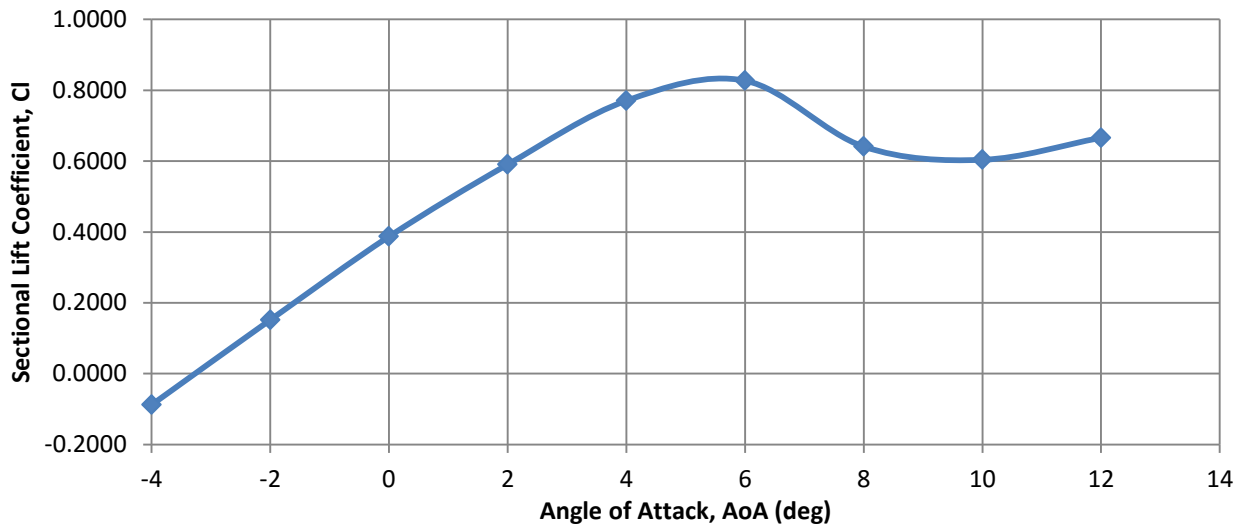


Figure 17: Sectional Force Coefficients of FX77-W-343 Airfoil (Baseline Case)

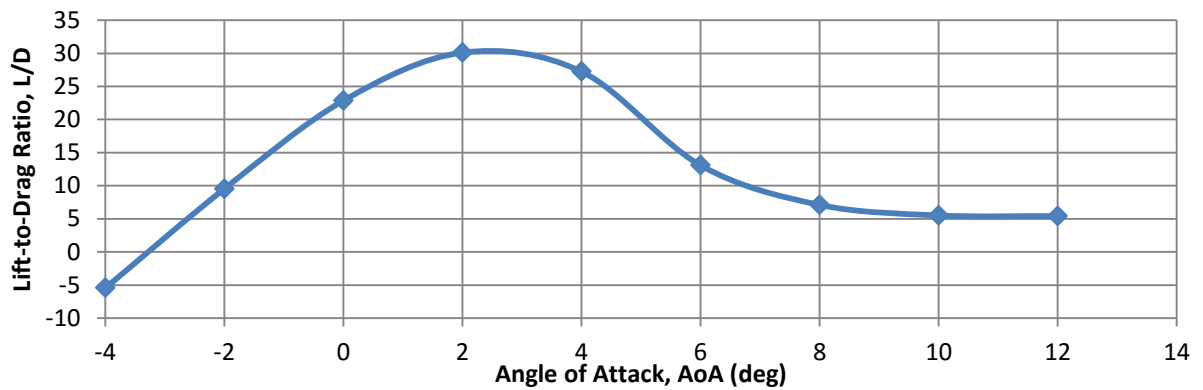


Figure 18: Lift-to-Drag Ratio of FX77-W-343 Airfoil (Baseline Case)

The above aerodynamic performance plots are consistent with the simulation flow field around the airfoil. These flow velocity field of -4° to 12° can be seen in Figure 19. As seen in the velocity field in all AoA, the flow velocity is highest near the maximum cambered region. Due the shape of the blunt airfoil trailing edge, vortexes can be found immediately aft of the airfoil. According to Grasso [8], the blunt or flat back trailing edge is a design philosophy used for exceptionally thick airfoil in attempt to improve the aerodynamic performance in terms of lift. At 4° and 6° AoA, the top surface of the airfoil showed sign of small separation near the trailing edge region. From AoA of 6° to 12° , large flow separation exists and lessens the aerodynamic performance of the thick airfoil.

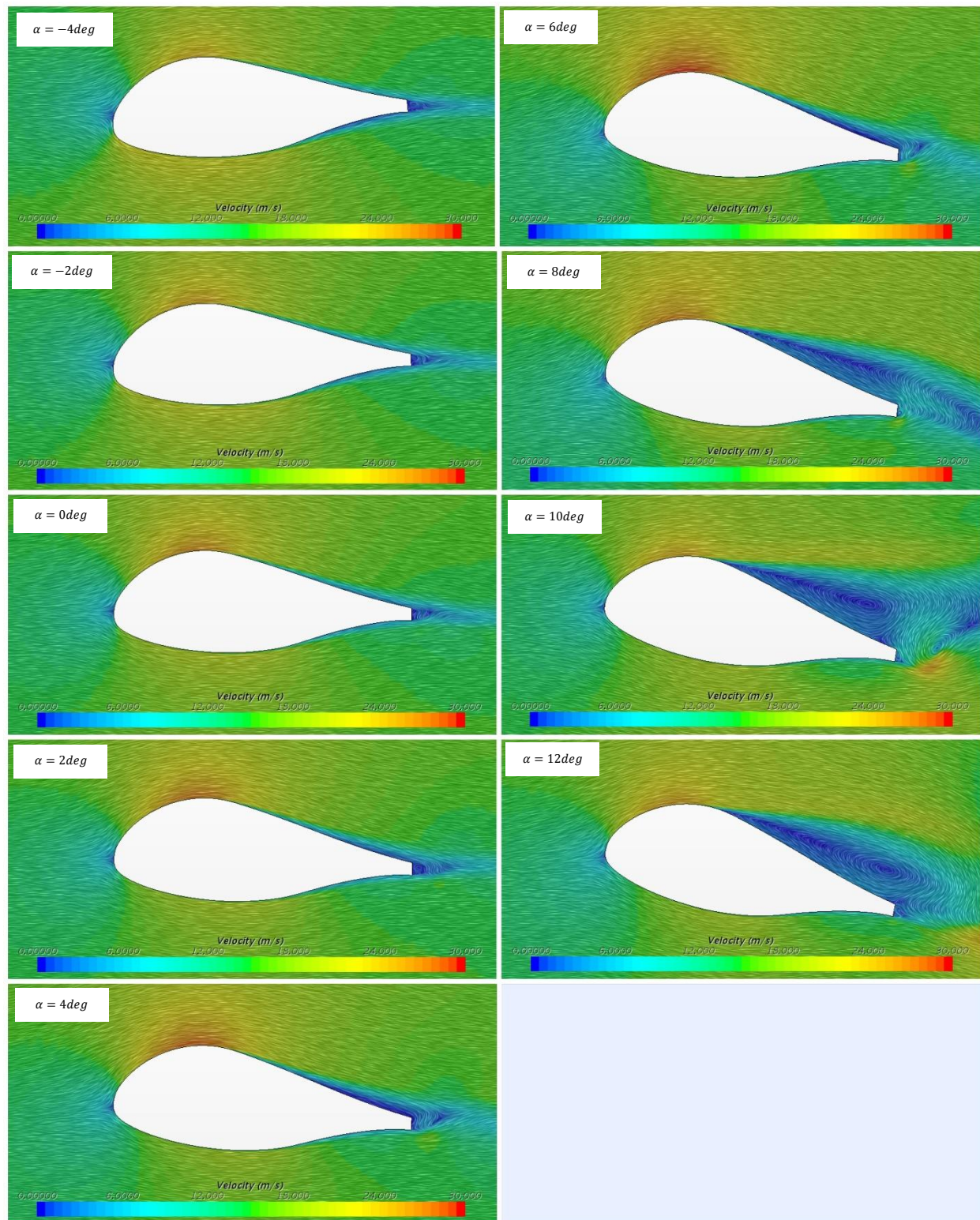


Figure 19: Velocity Flow Field over FX77-W-343 Airfoil from -4deg to 12deg (baseline Case)

Figure 20 presents static pressure contour on the baseline FX77-W-343 airfoil case at 0deg and 10deg AoA. As suggested by Figure 19, the higher flow velocity on the upper surface yields lower static pressure.

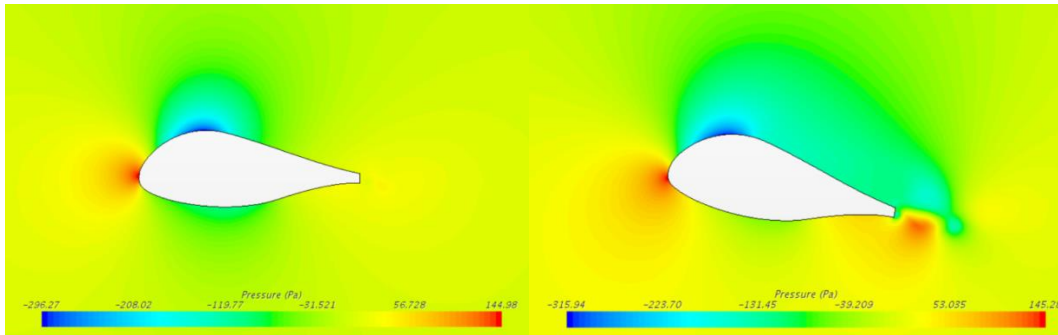


Figure 20: Static Pressure Contour on FX77-W-343 Airfoil at 0deg (right) and 10deg (right) AoA

Figure 21 presents the wake trail of extremely thick airfoil at 0deg and 6deg AoA. Similar to the wake generated by NREL S825 airfoil, the vorticity trail at 0deg is much weaker than 6deg AoA. At 6deg, the airfoil stalls and leaves behind massive wakes that contribute to high Sectional Drag Coefficient.

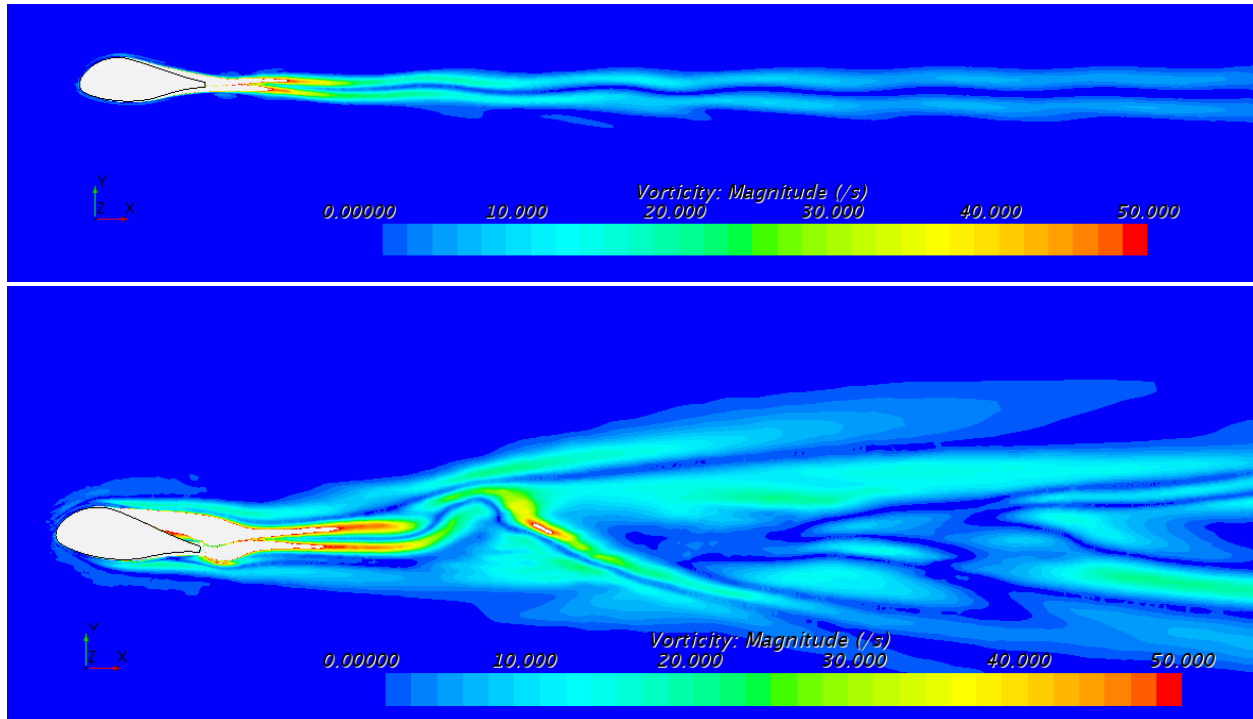


Figure 21: Vorticity Field on FX77-W-343 Airfoil at 0deg and 6deg AoA

4.2 Co-Flow Jet Modified FX77-W-343

The geometry of the exceptionally thick FX77-W-343 airfoil is modified to incorporate the air injection and suction slots. This is done by offsetting the top curve of the airfoil by 4mm or 0.4% thickness to chord ratio and excess section is removed. This means the injection and suction slot has the channel height of 4mm. Referring back to equation 3 and 4, the momentum jet coefficient can be calculated with this established slots height. Following the wind tunnel experiment of the co-flow jet airfoil conducted by University of Miami [17], the location of injection and suction provide the best performance at 8% and 85% chord, respectively. The location of the two slots on the upper surface of FX77-W-343 was created following the experimental results to achieve the best performance out of active flow control, co-flow jet. Figure 22 shows the modified geometry of the airfoil.

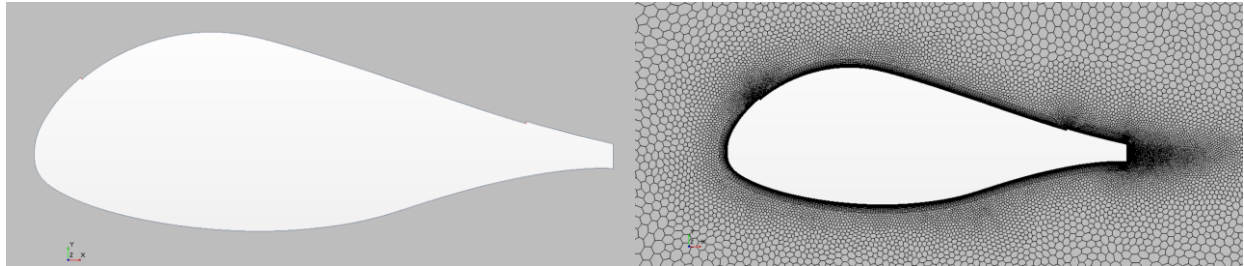


Figure 22: Co-Flow Jet Modified FX77-W-343 Airfoil Geometry (Left) and Mesh (right)

Based on the previous baseline simulation of the airfoil, the jet injection and suction air quantity study is conducted at 0deg and 6deg (AoA at maximum lift coefficient). The jet quantity or momentum jet coefficient ranging from 0.01 to 0.2 is studied for both AoA cases. For the investigation of co-flow jet in this document, the suction and injection momentum coefficients are established to be equal to each other for all cases. Figure 23 and Figure 24 demonstrates the effect of jet momentum coefficient to the aerodynamic performance parameters at 2 different AoA. The dashed line for the plots below represents the baseline value from previous section and therefore no injection or suction jet is applied.

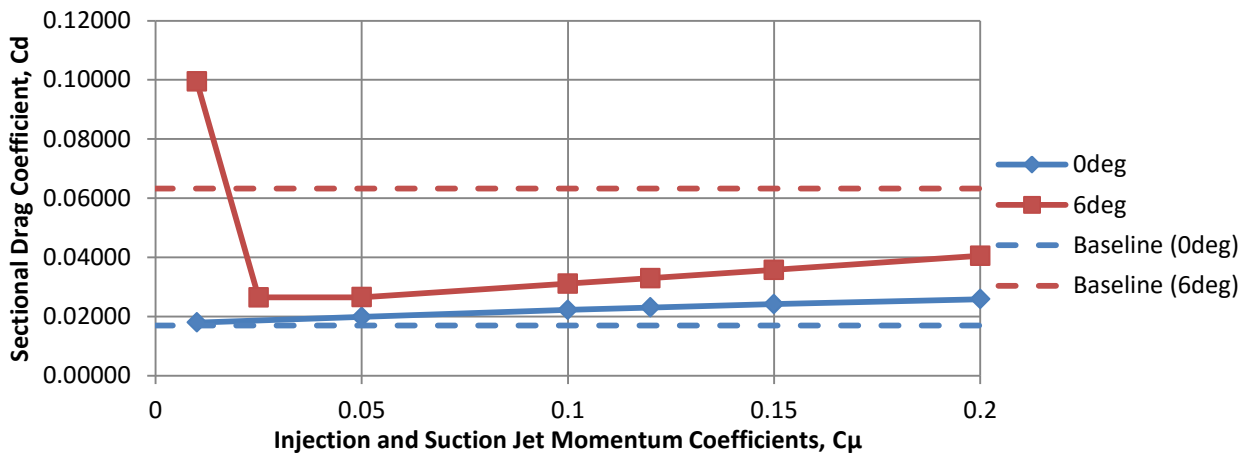
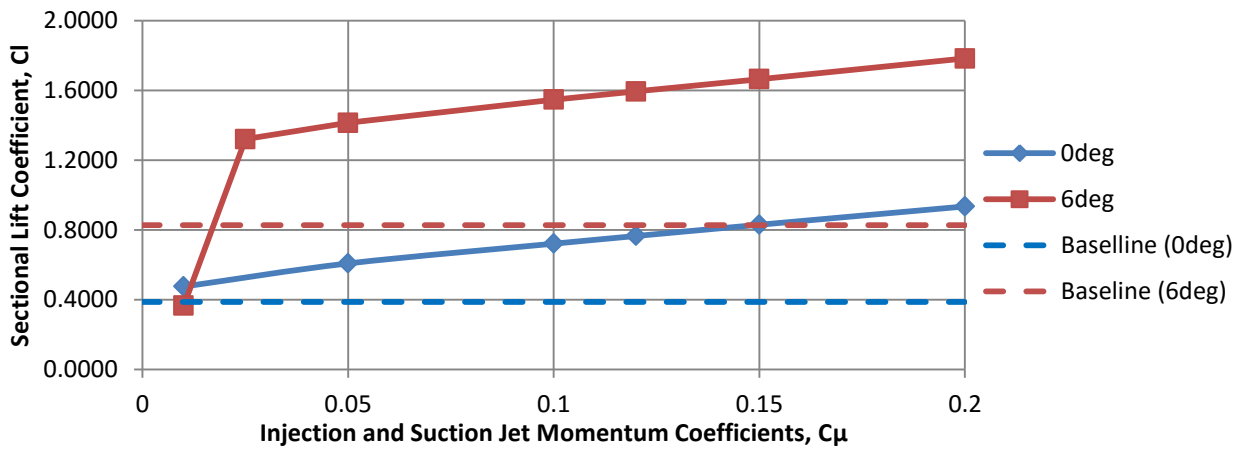


Figure 23: Injection and Suction Jet Momentum Coefficient versus Sectional Force Coefficient

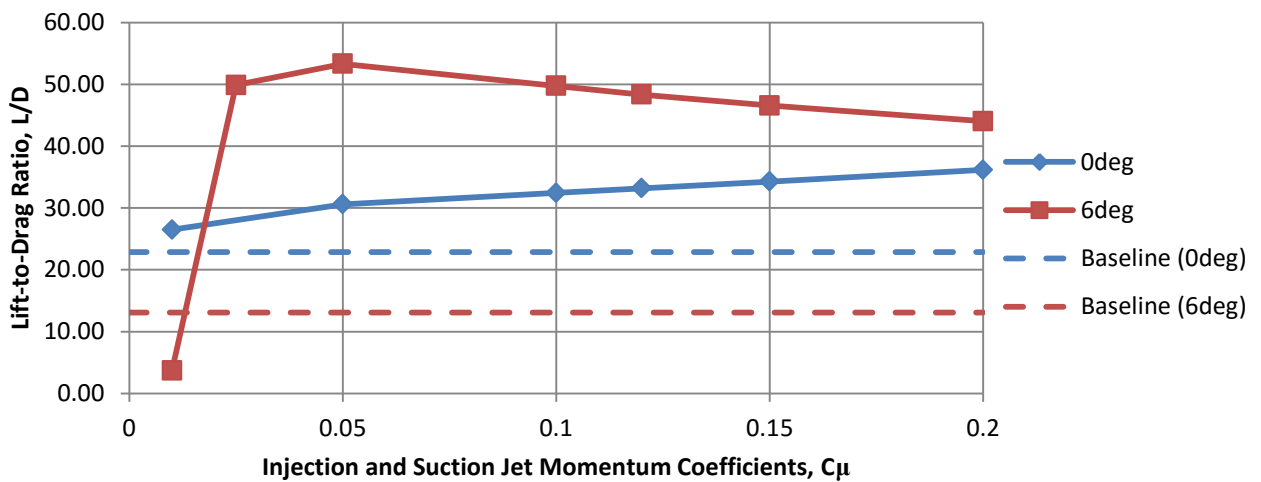


Figure 24: Injection and Suction Jet Momentum Coefficient versus Lift-to-Drag Ratio

The study in the above graphs shows 0deg AoA lift coefficient can be improved for even low jet momentum coefficient value. At the AoA of 6deg, small jet momentum of 0.01 does not prevent the flow from separating on the upper surface of the thick airfoil. The simulation result shows that a very low injection and suction quantity could in fact enhance the stall behavior, which results in lower lift and higher drag. From the force coefficient graph, it can be said that the lift and drag coefficient are improved as the jet momentum quantities increase, but this is not the reality according to wind tunnel data. According to the experimental results by the University of Miami [17], there is a limit to jet momentum coefficient to maintain the stability of the flow. At extremely high jet momentum value, the flow field around the airfoil breaks down, causing large separation and diminished aerodynamic performance of the airfoil.

The lift-to-drag ratio at 0deg case appears to increase as a function of jet momentum coefficient. At 6deg AoA, the lift-to-drag ratio seems to maximize when the co-flow jet momentum is 0.05, and slowly decreases as the jet quantity becomes larger. Based on the simulation of an airfoil at 0deg and 6deg, the jet momentum coefficient of 0.05 is selected because it enhanced the overall performance characteristic of an airfoil and contributed to maximum lift-to-drag ratio at 6deg AoA.

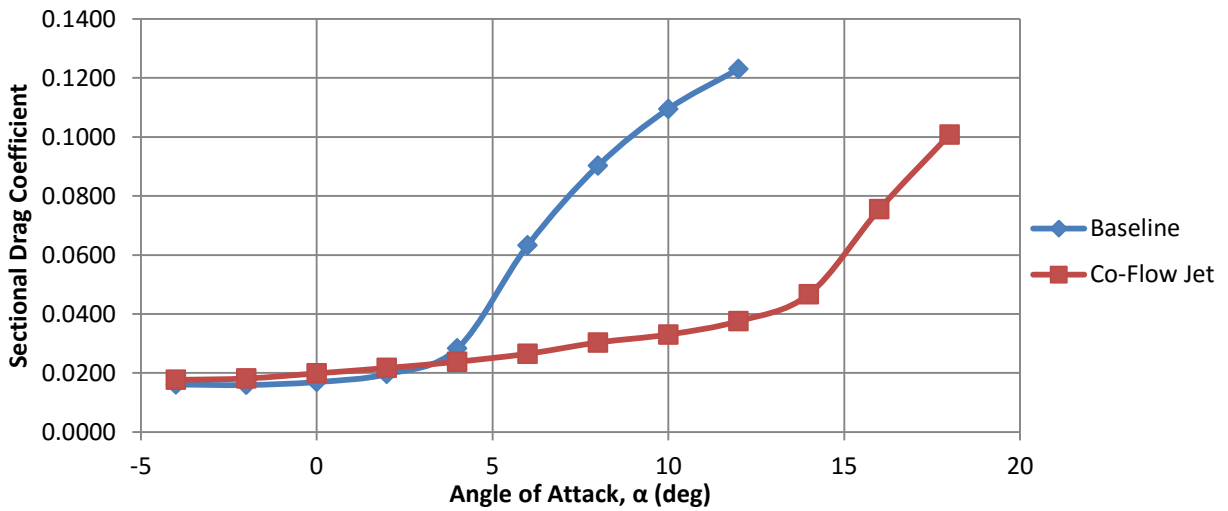
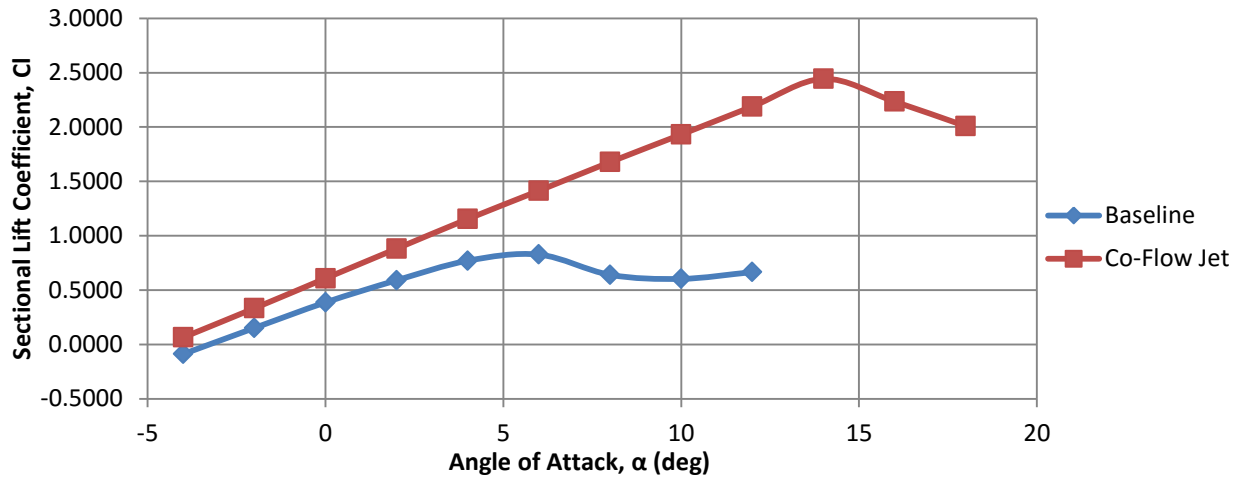


Figure 25: Sectional Force Coefficients Comparison between Baseline and Co-Flow Jet ($C_{\mu} = 0.05$)

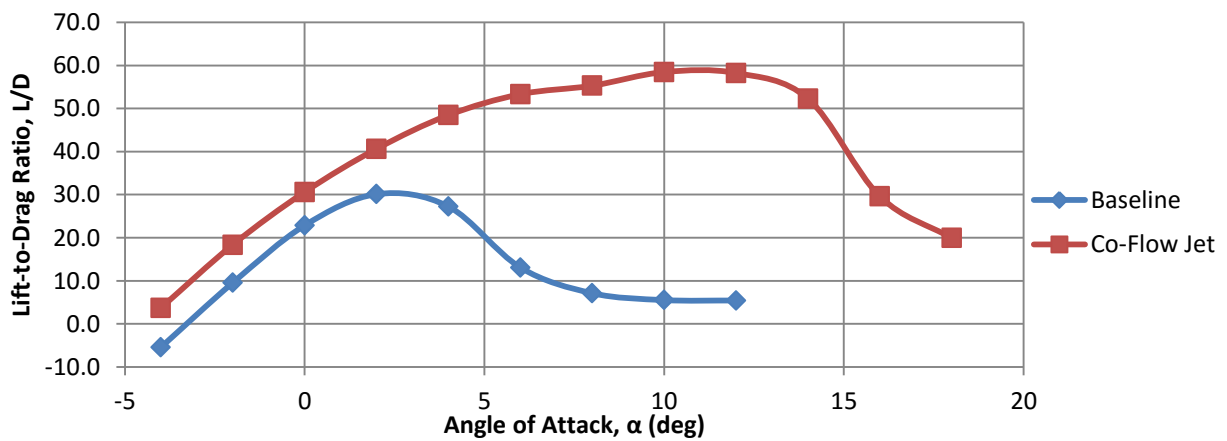


Figure 26: Lift-to-Drag Ratio Comparison between Baseline and Co-Flow Jet ($C_{\mu} = 0.05$)

From the above figures, the lift coefficient is improved from baseline for all AoA and stall is delayed from 6deg to 14deg. Although the stall AoA is delayed by 8deg, the unfavorable sharp stall behavior still exists. The maximum lift increases from 0.83 to 2.23, or about 190%. The active flow control, particularly co-flow jet, also enhanced the lift curve slope of the extreme thick airfoil by 22%, from 6.18rad^{-1} to 7.53rad^{-1} . At low angle of attack, the drag coefficient for co-flow jet case is higher but only by a small margin. The drag becomes smaller than the baseline case when flow on the upper surface starts to separate at AoA of 4deg. Even though the drag is higher for co-flow jet airfoil, the overall performance lift-to-drag ratio is still improved from the baseline case for all AoA. The lift-to-drag ratio is increased from 30.0 at 2deg to 58.5 at 10deg AoA, as seen in Figure 26. The significant improvement in both characteristic and performance values are consistent with the previous research conducted by engineers at the University of Miami. Figure 27 presents the velocity flow field around co-flow jet modified FX77-W-343 airfoil from -4deg to 18deg AoA.

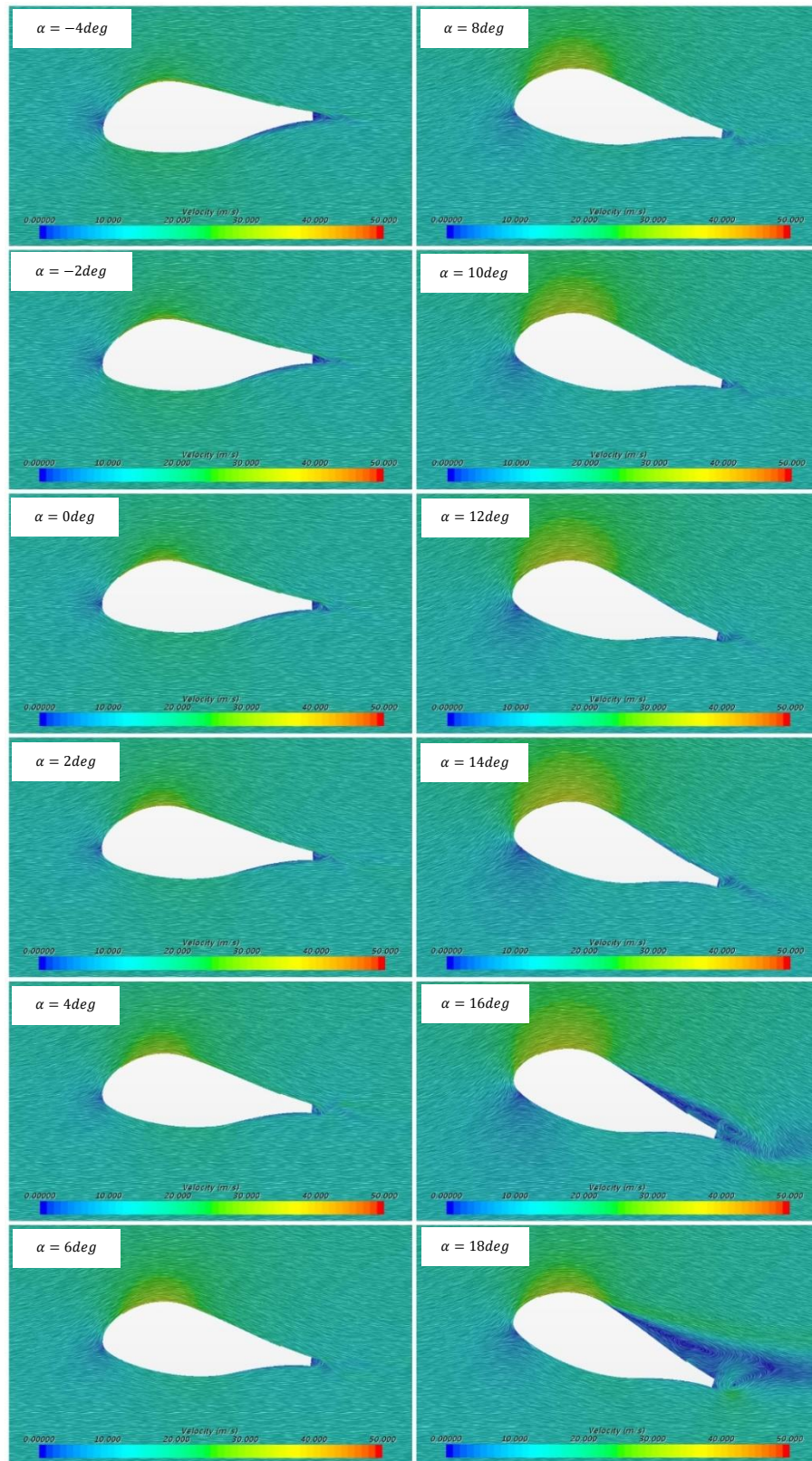


Figure 27: Co-Flow Jet Active Flow Control on FX77-W-343 Airfoil ($C_{\mu} = 0.05$)

Figure 28 presents the static pressure contour on the co-flow jet flow control ($C_{\mu} = 0.05$) airfoil at 0deg and 16deg AoA. At the two AoA cases, the static pressure is lower on the upper than the lower region.

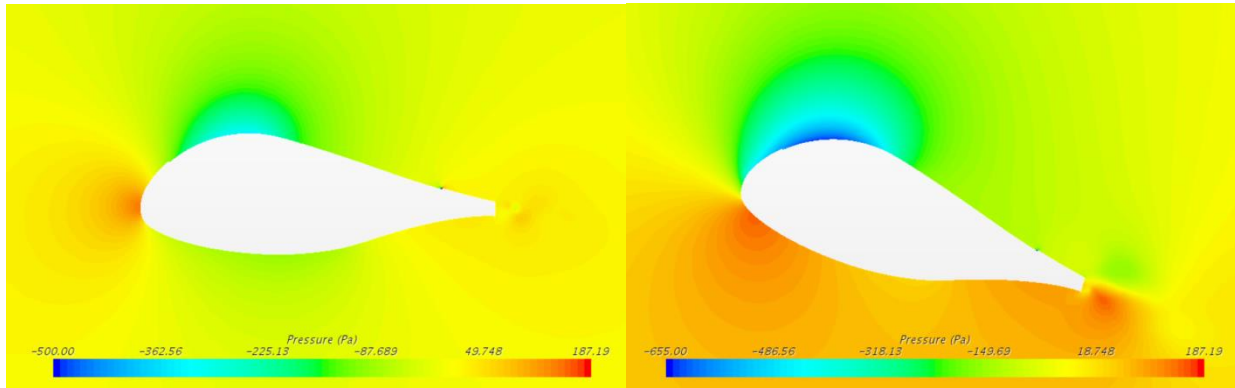


Figure 28: Static Pressure Contour on Modified FX77-W-343 airfoil at 0deg (left) and 16deg (right) AoA

Figure 29 show the enlarged flow fields near the injection and suction jet of $C_{\mu} = 0.05$ on the airfoil upper surface. The distinct differences between freestream and the injection flow velocity can be seen near the injection slot. The two flow streams velocity is mixed and enhanced the overall velocity close to the maximum cambered region. On the other side, the suction slot keeps the flow attached near the trailing edge. Low velocity flow can be found immediately aft of the suction location caused by the interaction between suction slot and the wall. It is suggested by the author that this interaction could be reduced by lowering the suction momentum coefficient.

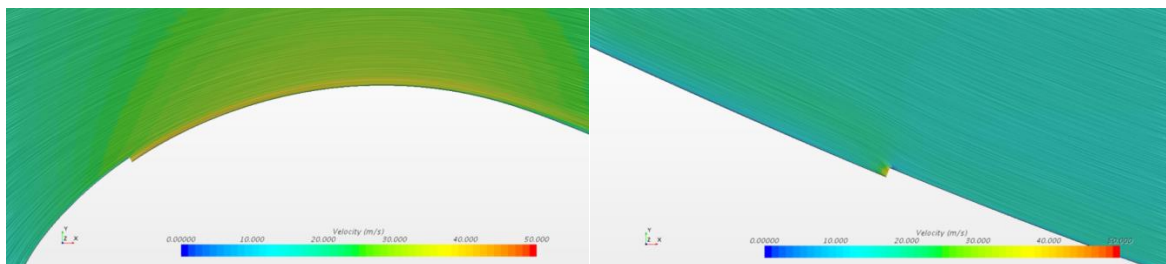


Figure 29: Velocity Flow Field near Leading Edge (left) and Trailing Edge (right) of Co-Flow Jet Flow Control FX77-W-343 Airfoil at 6deg AoA

The interaction between the injection and suction flow to incoming freestream can also be seen in the vorticity contour plot, Figure 30. The shear layer between freestream and the injection generated high intensity vorticity flow, which helps the flow stay attached to the aerodynamic body. Notice, the blunt trailing edge created vortex shedding behind the airfoil.

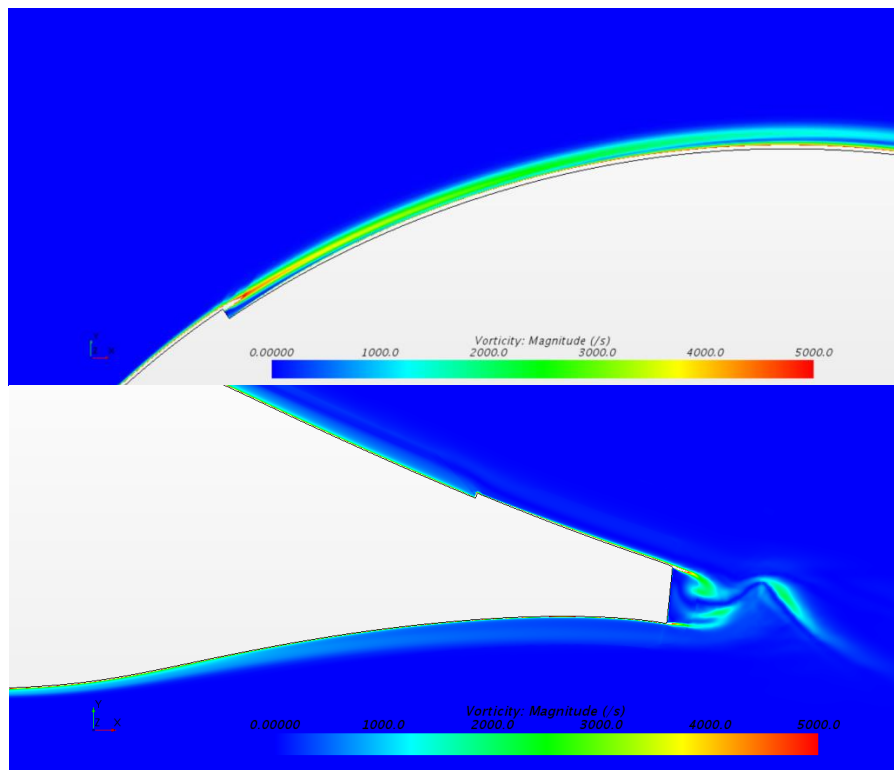


Figure 30: Vorticity Field near Leading Edge (top) and Trailing Edge (bottom) of Co-Flow Jet Flow Control FX77-W-343 Airfoil at 6deg AoA

Figure 31 examined the wake generated by co-flow jet active flow control FX77-W-343 Airfoil at 0deg and 16deg AoA. Consistent with the baseline case, the 0deg AoA airfoil generated thinner and weaker strength vorticity when compared to the stalled airfoil at 16deg AoA.

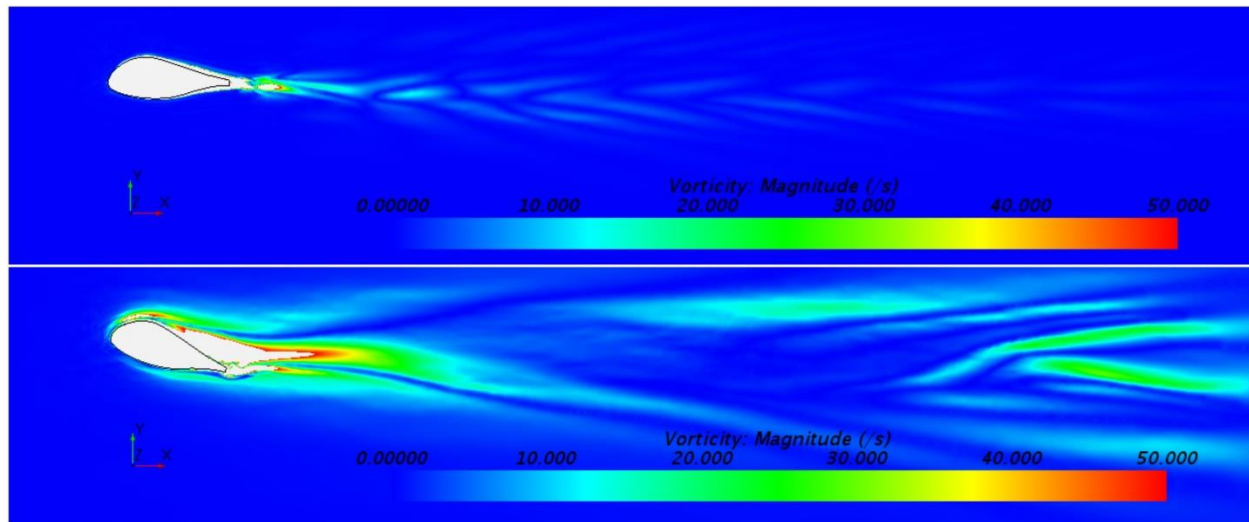


Figure 31: Vorticity Field on Co-Flow Jet Flow Control FX77-W-343 Airfoil at 0deg (Top) and 16deg (bottom) AoA

Figure 32 and Figure 33 present the vorticity field downstream of the 6deg AoA airfoil with various injections and suction momentum coefficient quantities at 6deg AoA. At the lowest setting of injection and suction momentum ($C_{\mu} = 0.01$), the flow separation appeared and generate a large and high-intensity wake trail. Momentum coefficient above 0.012 prevents the thick airfoil from stalling at 6deg AoA. As demonstrated in Figure 32 and Figure 33, the level of vorticity intensifies in the wake as the injection and suction jet momentum coefficient increases, which is consistent with the data provided in Figure 23 and Figure 24. At 6deg AoA with injection and suction momentum of 0.05, the extremely thick FX77-W-343 airfoil has the thinnest and lowest intensity wake structure, yielding the performance with lowest sectional drag coefficient and highest lift-to-drag ratio.

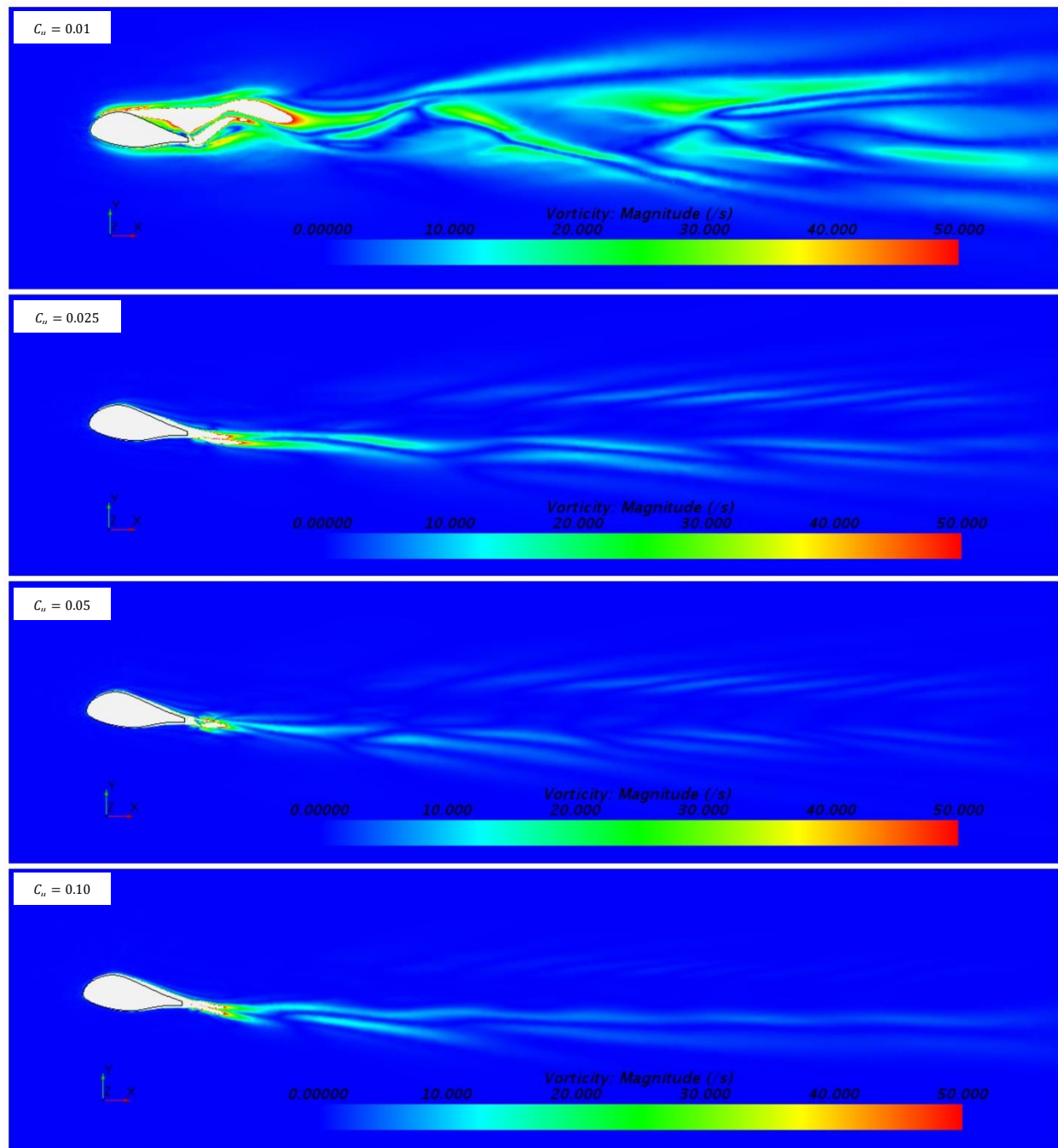


Figure 32: Comparison of the Wake Structure with Various Injection and Suction Momentum Coefficient on Co-Flow Jet Flow FX77-W-343 airfoil at 6deg AoA

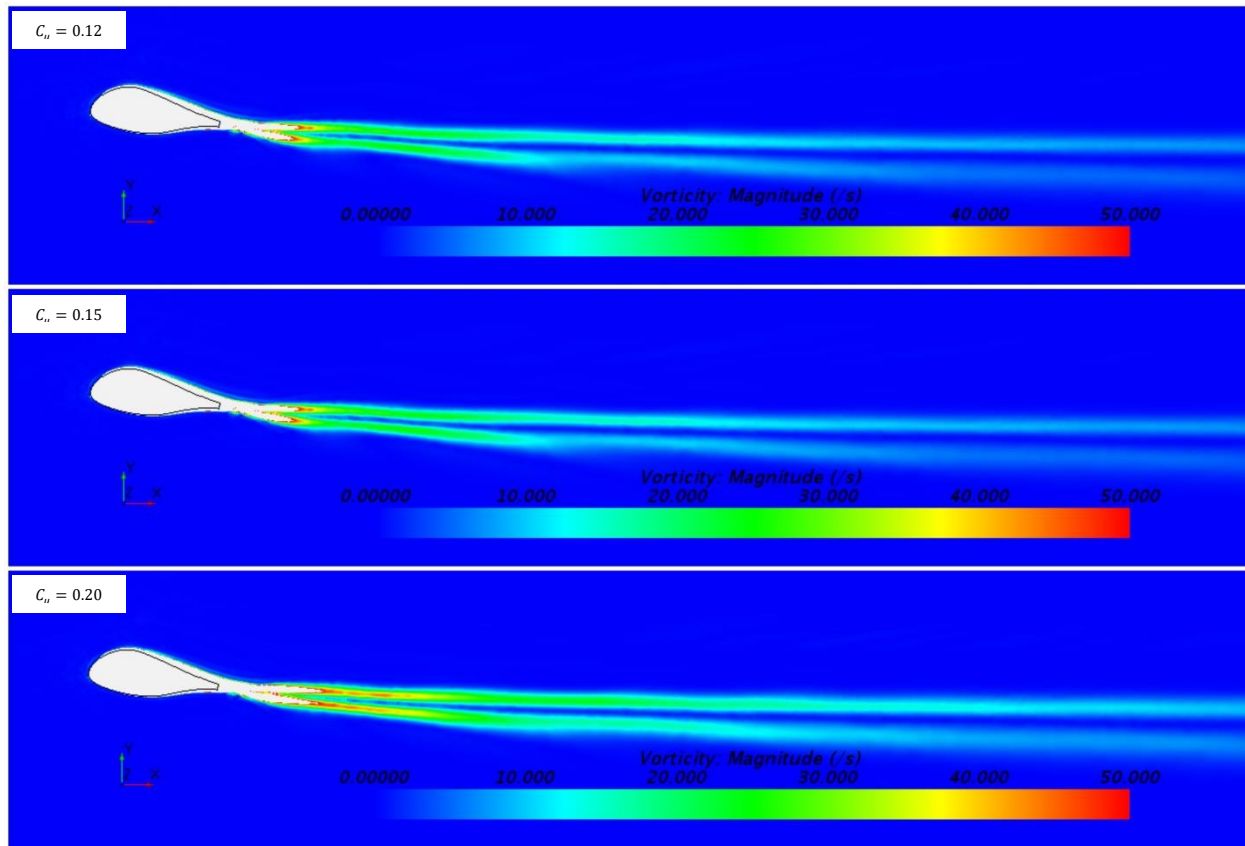


Figure 33: Comparison of the Wake Structure with Various Injection and Suction Momentum Coefficient on Co-Flow Jet Flow FX77-W-343 airfoil at 6deg AoA (continue)

Figure 34 demonstrates side-by-side comparison between flow field velocity of clean and modified FX77-W-343 airfoil. In the baseline case, flow separation occurred immediately aft of the maximum cambered. The co-flow jet with injection and suction slots keep the flow attached on the airfoil upper surface. The maximum flow velocity of the active flow airfoil is also higher, which suggests lower minimum static pressure. Figure 35 compares static pressure on baseline and co-flow jet airfoil at 6deg AoA. As suggested by the velocity field, the momentum and overall static pressure of the flow control airfoil is lower than the baseline case. The difference in pressure between upper and lower surface of the airfoil results in lift force. The comparison in Figure 34 and Figure 35 confirms the increase in performance of the co-flow jet active flow control.

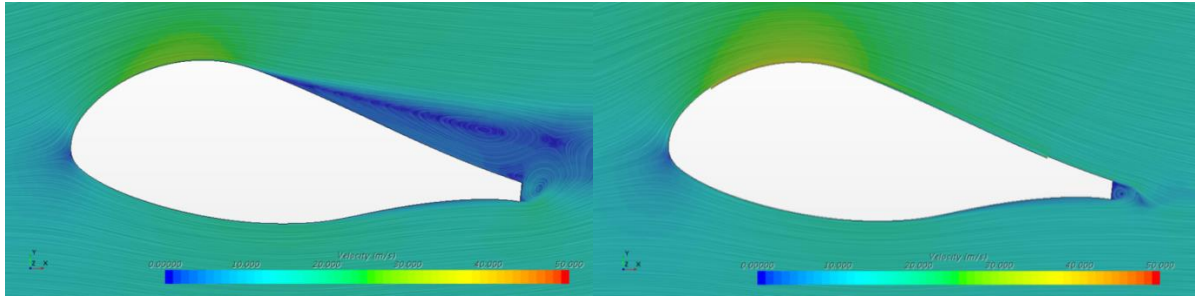


Figure 34: Comparison between Velocity Field on Baseline (left) and Modified Co-Flow Jet (right) FX77-W-343 Airfoil at 6deg AoA

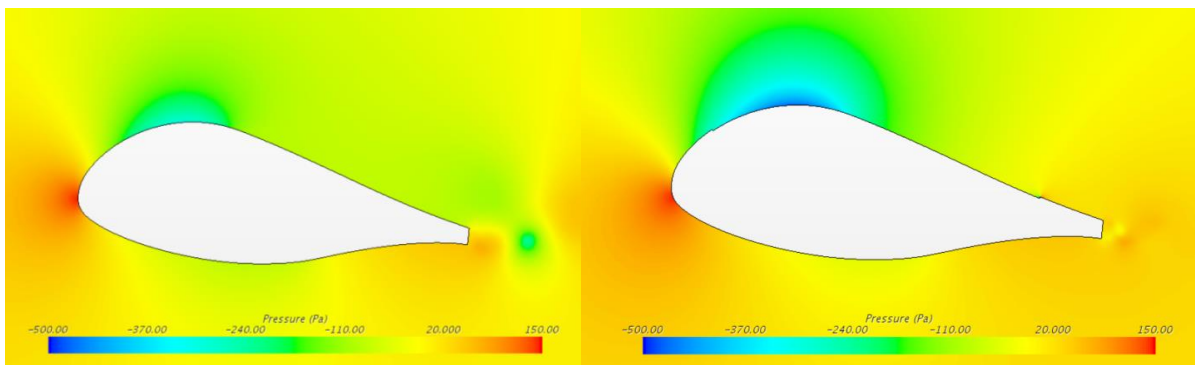


Figure 35: Comparison between Static Pressure Contour on Baseline (left) and Modified Co-Flow Jet (right) FX77-W-343 Airfoil at 6deg AoA

5 Conclusion and Recommendation

This Master Thesis documents the investigation of co-flow jet active flow control on 34.4% thick FX77-W-343 airfoil using STAR-CCM+. The geometry of the airfoil is created by connecting the top and bottom coordinate points using the spline curve feature in NX 8.5. The geometry is imported into STAR-CCM+ to create the flow domain. The field flow domain is meshed in 2-D with a polyhedral and prism layer mesher. The mesh sensitivity is performed for this airfoil case and is concluded that the domain must have at least 50,000 elements. For the physics model, RANS is selected to be the governing equations with constant density gas flow. The SST K-Omega turbulence model is chosen mainly because it performs well in adverse pressure gradients, or stall regions. The low wall y^+ treatment is applied in order to achieve accurate force coefficient results in low Reynolds simulations.

The validation simulation case is conducted at Reynolds number of 1,000,000 on NREL S825 airfoil instead of FX77-W-343 due to the availability of the experimental wind tunnel data. NREL S825 simulation result follows the behavior of the airfoil in the wind tunnel with acceptable sectional force coefficient values.

The simulation of FX77-W-343 airfoil is executed with the exact same mesh and physics settings as the validation case on NREL S825. The co-flow jet modified airfoil is chosen to have two slots with a height of 4mm at 8% and 85% chord. The injection and suction jet momentum coefficient is selected to be 0.05 and simulated in the 15.66m/s flow, or 1,000,000 Reynolds number. The co-flow jet active flow control made a significant improvement in terms of aerodynamic performance and behavior. The simulation showed that the maximum lift coefficient is increased by 190%, lift curve slope amplified by 22%, and maximum lift-to-drag ratio improved by 94%. Although the undesirable sharp stall behavior still persists, the operating margin has increased because stall AoA is delayed from 6deg to 14deg.

For future improvement in the study of co-flow jet active flow control related to wind turbine application, the study should be done to understand the relationship between the cost of injection and suction jet flow, and the return in terms of power being generated. The wind turbine equipped with co-flow jet flow control also should be modeled in 3-D CFD to see the effect of 3-D flow with the active flow control modification.

6 Reference

1. Anon. "UIUC Airfoil Coordinates Database," *UIUC Applied Aerodynamics Group*, University of Illinois Urbana-Champaign, Department of Aerospace Engineering, [Online], http://m-selig.ae.illinois.edu/ads/coord_database.html, [retrieved 26 April 2016].
2. Anon., "NREL's S825 Airfoil Graphic and Coordinates," *National Renewable Energy Laboratory*, October 2014, [Online], http://wind.nrel.gov/airfoils/shapes/S825_Shape.html, [retrieved 26 April 2016].
3. Anon., "Spotlight on Turbulence," *The Steve Portal*, February 2016, [Online], https://steve.cd-adapco.com/articles/en_US/FAQ/Spotlight-on-Turbulence [retrieved 26 April 2016].
4. Anon., "The Siemens D7 Platform," *Siemens*, [online], <http://www.energy.siemens.com/us/en/renewable-energy/wind-power/platforms/d7-platform/>, [retrieved 26 April 2016].
5. Anon., "User Guide," *STAR-CCM+*, CD-Adapco, [Online], http://stevedocs.cd-adapco.com/ViewDocs/authdocs/starccmplus_latest_en/index.html?param=8pGTb&authLoc=https%3A%2F%2Fsteve.cd-adapco.com%2FAuthoriseRedirect, [retrieved 26 April 2016].
6. Anon., "Wind Power's Beginnings (1000 B.C. – 1300 A.D.)," *Illustrated History of Wind Power Development*, [online], <http://telosnet.com/wind/early.html> [retrieved 26 April 2016].
7. Djojodihardjo, H., Abdulhamid, M. F., Basri, S., Romli, F. I., and Abdul Majid, D. L. A., "Numerical Simulation and Analysis of Coanda Effect Circulation Control For Wind-Turbine Application Considerations," *IJUM Engineering Journal*, Special Issue University of Pultra Malaysia (UPM), Department of Aerospace Engineering, 2011.
8. Grasso, F., "Development of Thick Airfoils for Wind Turbines," *Energy Research Centre of the Netherlands*, January 2012.
9. Nguyen, C., "Incompressible Case," *Turbulence Modeling*, [online], http://www.mit.edu/~cuongng/Site/Publication_files/TurbulenceModeling_04NOV05.pdf, [retrieved 26 April 2016].

10. Penny, C., “Subsonic Wing Simulation Tutorial and Best Practices,” *The Steve Portal*, CD-Adapco, May 2014, [Online Video], https://steve.cd-adapco.com/articles/en_US/Video/Subsonic-Wing-Simulation-Tutorial-and-Best-Practices [retrieved 26 April 2016].
11. Piperas, A. T., “Investigation of Boundary Layer Suction on a Wind Turbine Airfoil using CFD,” *DTU Mechanical Engineering*, Department of Mechanical Engineering, Denmark, August 2010.
12. Raina, A. A., Lee, K. T., Wetzel, K. K., “Optimization and Design of a 105m Blade for a 10MW Hurricane-Resilient Wind Turbine,” *33rd Wind Energy Symposium*, Kissimmee, Florida, 2015.
13. Raina, A. A., Wetzel, K. K., Farokhi, S., “Modeling and Simulation of a 3MW Wind Turbine Blade for Determination and Analysis of flow characteristics,” *33rd Wind Energy Symposium*, Kissimmee, Florida, 2015.
14. Shapiro, A. H., “Film Notes for Vorticity,” *National Committee for Fluid Mechanics Films*, Massachusetts Institute of Technology, Cambridge, Massachusetts, 1969.
15. Somers, D. M., “Design and Experimental Results for the S825 Airfoil,” *National Renewable Energy Laboratory*, Golden, Colorado, 1999, [Online], <http://www.nrel.gov/docs/fy05osti/36346.pdf>, [retrieved 26 April 2016].
16. Zha, G. Gao, W., and Paxton, C., “Numerical Simulation of Co-Flow Jet Airfoil Flow,” *AIAA Aerospace Sciences Meeting and Exhibit 2006*, University of Miami, Department of Mechanical and Aerospace Engineering, 2006.
17. Zha, G., Carroll, B. F., “High Performance Airfoil Using Co-Flow Jet Flow Control,” *AIAA 2005*, University of Miami, Department of Mechanical and Aerospace Engineering, 2005.